On the Contribution of Fast and Slow Responses to Precipitation Changes Caused by Aerosol Perturbations

Shipeng Zhang[1], Philip Stier[1], Duncan Watson-Parris[1]

[1] Atmospheric, Oceanic and Planetary Physics, Department of Physics, University of Oxford, UK

Correspondence to: Shipeng Zhang (shipeng.zhang@physics.ox.ac.uk)

Abstract. Changes in global-mean precipitation are strongly constrained by global radiative cooling, while regional rainfall changes are less constrained because energy can be transported. Absorbing and non-absorbing aerosols have different effects on both global-mean and regional precipitation, due to the distinct effects on energetics. This study analyses the precipitation responses to large perturbations in black carbon (BC) and sulphate (SUL) respectively by examining the changes in atmospheric energy budget terms on global and regional scales, in terms of fast (independent of changes in sea surface temperature (SST)) and slow responses (mediated by changes in SST). Changes in atmospheric radiative cooling/heating are further decomposed into contributions from clouds, aerosols, and clear-clean sky (without clouds or aerosols).

Both cases show a decrease in global-mean precipitation, dominated by fast responses in the BC case while slow responses in the SUL case. The geographical patterns are distinct too. The intertropical convergence zone (ITCZ), accompanied with tropical rainfall, shifts northward in the BC case, while southward in the SUL case. For both cases, energy transport terms from the slow response dominates the changes in tropical rainfall, which are associated with the northward (southward) shift of Hadley cell in response to the enhanced southward (northward) cross-equatorial energy flux caused by increased BC (SUL) emission. The extra-tropical precipitation decreases in both cases. For the BC case, fast responses to increased atmospheric radiative heating contribute most to the reduced rainfall, in which absorbing aerosols directly heat the mid-troposphere, stabilise the column, and suppress precipitation. Unlike BC, non-absorbing aerosols decrease surface temperatures through slow processes, cool the whole atmospheric column, and reduce specific humidity, which leads to decreased radiative cooling from the clean-clear sky, and is consistent with the reduced rainfall. Examining the changes in large-scale circulation and local thermodynamics qualitatively explains the responses of precipitation to aerosol perturbations, whereas the energetic perspective provides a method to quantify their contributions.

1. Introduction

Aerosols have been proposed to affect clouds and precipitation to a large extent by interacting with clouds and radiation (Ramanathan et al., 2001). However, aerosol effects on clouds and precipitation remain highly uncertain due to the complex nature of aerosol-cloud-radiation interactions. For example, satellite-estimated and model-simulated aerosol-cloud interactions show large discrepancies in terms of magnitude and even in sign (e.g. Ackerman et al., 2004; Rosenfeld et al., 2019; Wang et al., 2012). Disagreements between different studies can be attributed to methodologies (Gryspeerdt et al., 2014), model uncertainties (White et al., 2017) and, importantly, are often related to differences in environmental conditions, such as relative humidity, dynamic background, cloud types, stability (Alizadeh-Choobari, 2018; Khain, 2009; Khain et al., 2008; Lohmann et al., 2007; Zhang et al., 2016). Knowledge about the chain of processes, from aerosol emission to acting as cloud condensation nuclei (CCN) or ice nuclei (IN) and to cloud microphysics and dynamics, is critical for reducing the uncertainties and understanding the climate system (Ghan et al., 2016), which is referred to as a 'bottom-up' approach. However, this is challenging, considering uncertainties can arise from aerosol emissions, activation, cloud microphysics and dynamic regimes (e.g., Gettelman et al., 2013; Ghan et al., 2012; Michibata et al., 2016; Zhang et al., 2016).

An energetic perspective provides an alternative approach to examine aerosol effects on precipitation, which is referred to as a 'top-down' approach. For global scales, in equilibrium, latent heat released from rainfall should be energetically balanced by atmospheric radiative cooling together with surface energy fluxes (Allen and Ingram, 2002; Andrews et al., 2010). Climate forcers, such as greenhouse gases (GHGs) and aerosols, which affect the energy budget, can modify the hydrological responses (Kvalevåg et al., 2013; Stephens and Hu, 2010). The energy constraints can be applied to regional rainfall by introducing the energy transport term (H) (Muller and O'Gorman, 2011; Richardson et al., 2016). The local energy budget at equilibrium can be addressed as the following equation:

$$L\delta P = \delta Q + \delta H \tag{1}$$

where δ denotes the difference between two climate states (e.g., with and without anthropogenic aerosols). L refers to the latent heat of condensation, and P is the precipitation rate, so LP refers to the atmospheric latent heating rate from rainfall. H is the column-integrated divergence of dry static energy which is expected to be zero on a global scale. Q is the atmospheric diabatic cooling (except for latent heat released from precipitation), consisting of atmospheric radiative cooling (ARC) and downward surface sensible heat flux (-SH). ARC is the difference of shortwave (SW) and longwave (LW) fluxes between top of the atmosphere (TOA) and the surface. ARC has significant impacts on global hydrological sensitivity (Allen and Ingram, 2002), while changes in the energy transport term (δH) are essential in determining the spatial pattern of precipitation response (Muller and O'Gorman, 2011). Dagan et al., (2019b) further demonstrated that whether precipitation responses are more correlated with changes in Q or H depends on the latitude considered. In the extra-tropics, diabatic cooling/heating perturbations are confined to local scales due to strong Coriolis force (thus weak energy transport), and hence the latent heating must balance diabatic cooling according to the energy budget. However, in the tropics, horizontal gradients of dry static energy are small due to the weak Coriolis force. Therefore, local strong diabatic heating perturbations can lead to thermally direct circulations that drive convergence/divergence of moisture and dry static energy. This low-level convergence of mass and moisture can lead to vertical motion and thus an increase in precipitation. So rainfall does not necessarily have to positively correlate with diabatic cooling (Dagan et al., 2019b).

69 Absorbing and non-absorbing aerosols can have different effects on each energy budget term, and thus
70 precipitation. On the global scale, black carbon (BC), a strongly absorbing aerosol, can stabilise the atmosphere
71 and suppress precipitation via strong shortwave absorption for short timescales, but also can increase precipitation
72 by warming up the surface temperature on longer timescales (e.g., Pendergrass and Hartmann, 2012). The net
73 effect can be uncertain among GCMs (Samset et al., 2016), and is sensitive to the altitude where the BC are added
74 (Ming et al., 2010). Unlike BC, non-absorbing aerosols, for example sulphate (SUL), reduce precipitation
75 predominantly by decreasing SST on long timescales through the dimming effect, whereby SUL scatters incoming
76 solar radiation back to the space (Boucher et al., 2013; Kasoar et al., 2018). Additionally, the surface sensible heat
77 flux is more sensitive to changes in BC than SUL (Myhre et al., 2018; Richardson et al., 2018). On zonal scales,
78 due to the relatively short lifecycle of aerosols, the radiative forcing caused by aerosols is hemispherically
79 asymmetric, which leads to a warmer northern hemisphere for the BC case and colder one for the SUL case,
80 respectively. As a result, the cross-equatorial energy fluxes lead to the intertropical convergent zone (ITCZ)
81 shifting towards the warmer hemisphere (Wang, 2009; Bischoff and Schneider, 2016; Zhao and Suzuki, 2019;
82 Keshtgar et al., 2020; Zanis et al., 2020). On regional scales, it is also worth noting that SUL is usually more
83 suitable as CCN due to its higher hygroscopicity as compared to BC. It can therefore alter cloud microphysics
84 and subsequent precipitation formationregional rainfall by interacting with clouds. However, the susceptibility of
85 precipitation to sulphate aerosols (and the precursors) shows large discrepancies in satellite-estimated
86 precipitation susceptibility to aerosols from several products (Bai et al., 2018; Haynes et al., 2009), and a broad
87 inter-model spread (uncertainty) in GCMs (Ghan et al., 2016; Samset et al., 2016). Some studies also found that
88 the sensitivity of precipitation to sulphate aerosols variesdiffers between model-simulated and satellite-estimated
89 results, in terms of magnitude and sometimes in sign (Liu et al., 2020; Wang et al., 2012).

90 These responses of precipitation have been conventionally suggested to be composed of fast and slow responses
91 (Andrews et al., 2009; Bala et al., 2010). Fast responses, on the timescale from days to months, are independent
92 of changes in sea surface temperature (SST), and mostly dependent on instantaneous changes in atmospheric
93 radiative heating/cooling (O'Gorman et al., 2012; Richardson et al., 2016). It should be noted that even though
94 SST is unchanged in atmosphere-only models, the land surface temperature is generally still allowed to vary
95 (Stjern et al., 2017). Slow responses, on the timescale of years, are mediated by changes in sea surface temperature
96 (SST) and strongly correlate with top-of-atmosphere (TOA) forcing (Kvalevåg et al., 2013; Lambert and Webb,
97 2008; Suzuki et al., 2017). Distinguishing contributions from fast and slow responses are essential for
98 understanding the mechanisms that cause the precipitation changes. For example, Bony et al., (2013) examined
99 the responses of tropical rainfall to increasing GHGs. They found that the fast processes weaken the vertical
100 motion and counteract a considerable part of the increasing trend induced by surface warming. Shaw and Voigt
101 (2015) have investigated predicted changes in the summertime Asian monsoon under a warming scenario caused
102 by GHGs, and the fast responses caused by direct radiative effect are generally opposite to the slow impacts caused
103 by the SST warming. The changes in circulation are essential for local climate responses, including clouds,
104 radiation and precipitation (Johnson et al., 2019), whereas the spatial distribution of aerosols radiative forcing in
105 turn affects atmospheric circulations (Chemke and Dagan, 2018).

106 Distinguishing contributions from different energetic terms is also helpful for understanding physical processes
107 and model differences (DeAngelis et al., 2015). It has historically been used to distinguish contributions from
108 clouds and aerosols when studying aerosol radiative forcing (Forster et al., 2007; Ghan 2013). While energetics

109 have been applied before to analyse precipitation responses (e.g., Ming et al., 2010; Dagan et al., 2019b), here we
110 further decompose them into individual terms to provide additional insights. Changes in the energy transport term
111 (δH) can be decomposed into eddy and mean state components, which are further associated with changes in
112 thermodynamics and dynamics (Muller and O'Gorman, 2011; Richardson et al., 2016). Changes in ARC can be
113 further decomposed into contributions from aerosol (mostly through SW absorption), clouds (LW radiative
114 cooling), and clear-clean sky (mainly from water vapour, greenhouse gases, and the Planck feedback). While it
115 has long been appreciated that changes in ARC are essential in balancing latent heat release from precipitation
116 responses on global scales, their relationship on zonal mean or regional scales (and which ARC component
117 dominates) has not been fully explored.

118 The Precipitation Driver Response Model Intercomparison Project (PDRMIP) (Myhre et al., 2017) has conducted
119 several experiments to study the response of precipitation to different climate forcers, such as GHGs, aerosols,
120 and solar radiation change (e.g., Samset et al., 2016, Stjern et al., 2018). It has been found that the fast response
121 dominates the global-averaged precipitation responses to BC perturbation, which differs from other drivers of
122 climate change (Samset et al., 2017; Stjern et al., 2017). It has also been shown that BC contributes to the most
123 substantial uncertainties among GCMs in simulating the changes in surface temperature and precipitation, due to
124 different parameterisations of physical, chemical, and dynamical processes involved on the path from BC
125 emission to the final climate impact (e.g., Stjern et al., 2017). However, it is worth noting that most PDRMIP
126 research focuses on global mean changes and addressing uncertainties among GCMs (e.g., Myhre et al., 2017;
127 Richardson et al., 2018; Stjern et al., 2018). Samset et al., 2016 showed the spatial patterns of fast, slow and total
128 responses of precipitation to different climate forcers including absorbing and non-absorbing aerosols, with a
129 greater focus on the inter-comparison between different GCMs and different climate forcers. Here we study the
130 fast and slow response contribution to total response of precipitation with a focus on the comparison between
131 absorbing and non-absorbing aerosols, and in particular on the underlying mechanisms causing the differences by
132 distinguishing contributions from each energetic term at various scales.

133 In light of previous work illustrating the potential of energy budget constraints for understanding regional
134 precipitation changes, and the fact that absorbing and non-absorbing aerosols impact the response on two distinct
135 timescales, we aim to answer three questions: 1. What are the contributions of fast and slow responses to total
136 precipitation changes on global and regional scales? 2. What is the dominant energetic term in precipitation
137 responses to absorbing/non-absorbing aerosol perturbations on different spatial and temporal scales? 3. How to
138 relate changes in local thermodynamics and large-scale circulation to changes in energetic terms and quantify
139 their contribution to precipitation responses?

140 **2. Method**

141 The global aerosol-climate model ECHAM6-HAM2 (Stier et al., 2005, Zhang et al., 2012, Tegen et al., 2019,
142 Neubauer et al., 2019) is used to perform all the experiments. It is based on the general circulation model
143 ECHAM6 (Stevens et al., 2013) and is coupled to the aerosol module HAM2 (Stier et al., 2005; Zhang et al.,
144 2012). A two-moment cloud microphysics schemes is used to prognostically predict the number and mass mixing
145 ratios for both cloud water and ice (Lohmann et al., 2007; Lohmann and Hoose, 2009). The parametrisations for
146 convection, including cumulus convection and deep convections, are based on the scheme by Tiedtke (1989) and

147   Nordeng (1994). The activation of CCN to cloud droplets is adopted from Abdul-Razzak and Ghan (2000), which
148   is based on Köhler theory (Köhler, 1936). It should be noted that freshly emitted BC is assumed hydrophobic and
149   does not act as cloud condensation nuclei. However, subsequent condensation of sulfuric acid and mixing with
150   hydrophilic sulphate aerosols will increase its hygroscopicity so that internally mixed BC particles can activate as
151   CCN (Stier et al., 2006). In HAM2.3, BC can act as ice nuclei through heterogeneous freezing, but only in the
152   accumulation and coarse mode (Neubauer et al., 2019). The parameterisation for autoconversion is from
153   Khairoutdinov and Kogan (2000). There are 16 spectral shortwave bands in the solar radiation scheme, and 14
154   spectrum bands in the longwave radiation scheme (Pincus and Stevens, 2013). The general circulation model
155   ECHAM6 provides essential meteorological backgrounds such as temperature, pressure, wind and humidity,
156   which is coupled to HAM2 for the parameterisations of several aerosol processes such as aerosol activation and
157   deposition.

158   Emissions of anthropogenic BC, organic carbon and sulphate are from the Atmospheric Chemistry and Climate
159   Model Intercomparison Project (ACCMIP) emission dataset (Lamarque et al., 2010), including emissions from
160   industry, agriculture, aircraft, domestic, ships, and waste. Biomass burning emissions are also from ACCMIP
161   dataset, including both natural and anthropogenic biomass burning (Lamarque et al., 2010). Dimethyl sulphide
162   (DMS) emission is interactively related to the 10-meter wind speed and concentration in seawater. Biogenic
163   volatile organic carbon, and volcanic emissions are following the AeroCom phase II emission dataset (Dentener
164   et al., 2006). All the emissions are prescribed for the year 2000, so there are no interannual variabilities of
165   emissions. Simulations are performed at T63 (1.9° ×1.9°) spectral resolution using 47 vertical levels (L47).

166   To study the precipitation response to absorbing and non-absorbing aerosol perturbations, we analyse two
167   scenarios: one with a ten-times increase in BC emissions and another with a five-times increase in sulphur dioxide,
168   relative to baseline emissions in the year 2000 (Tegen et al., 2019). It should also be noted that the increases of
169   BC emissions here include both anthropogenic and natural sources. This is because the biomass burning emission,
170   as a large source of BC, includes both anthropogenic and emissions (e.g. agricultural waste burning) and naturally
171   occurring wild fire emissions. The anthropogenic contribution to wildfire emissions is assumed to dominate but
172   subject of significant uncertainties (e.g. Lamarque et al., 2010; van Marle et al., 2017). and it is very uncertain to
173   separate anthropogenic contribution of wild-fires. However, the increases in SO2 emissions are all anthropogenic
174   because the sources of volcanic and sulphur are kept the same. The main purpose of this work is to better
175   understand the mechanisms of aerosol-precipitation interactions, with a focus on, but not limited to, anthropogenic
176   aerosol effects. As only particular aerosol emissions are changed in each perturbation, the differences between
177   baseline and the perturbed case can be interpreted as aerosol effects. Geographical patterns of emission aerosol
178   optical depth change can be found in the supplementary file (Figure S1). We chose the multipliers of aerosol
179   emissions differently here is to make the aerosol effects statistically large enough and keep their radiative forcing
180   at the same magnitude (Myhre et al., 2017). Another reason is to make our results comparable with PDRMIP
181   work (Samset et al., 2016).

182   We run the simulations for 100 years with a mixed layer ocean (MLO), which is described as 50 meters in depth
183   (Dallafior et al., 2016). The ocean heat transport term (also known as the Q flux) is prescribed, which also means
184   the ocean dynamics are unchanged. Therefore, the changes in SST are caused by local responses to net surface
185   heat flux, and the responses in ocean circulations are omitted. To obtain the equilibrium state of precipitation
186   responses to aerosol perturbations, i.e. the total response (ΔP_{total}), we use the last 50 years of the simulations

187 because at that time the model has reached approximate equilibrium (Samset et al., 2016). We acknowledge that
188 it might take more than 100 years for a slab ocean model to fully equilibrate. Therefore we also performed a
189 Gregory-style regression (Gregory and Webb, 2008) to check the equilibrium for the BC and SUL cases
190 respectively (see supplementary file). For the BC experiment, it is very likely to reach equilibrium is reached
191 approximately after 50 years. For the SUL case, the energy imbalance is significantly reduced and reaches a near-
192 equilibrium after 50 years run as well, but it is suggested that more than 100 years simulation is needed to fully
193 equilibrate. So the total response of surface temperature to 5 times SUL should be even lower (more negative).
194 Considering the purpose of our study is to understand the mechanisms of precipitation responses to aerosols, an
195 exact equilibrium is not critical here and our conclusions still apply to an approximate equilibrium. Another
196 simulation is run for 20 years with fixed sea surface temperatures (fSST) and last ten years are used. The
197 precipitation responses for fSST simulations can be interpreted as the fast response (ΔP_{fast}). The slow response
198 is then calculated as the difference between the total response and the fast response (Myhre et al., 2017; Samset
199 et al., 2016):

200 $$\Delta P_{slow} = \Delta P_{total} - \Delta P_{fast} \tag{2}$$

201 The length of integration period is sufficient to derive the fast and total responses because the fast response of
202 precipitation occurs on time scales from days to months and a slower response on a time scale of years (Myhre et
203 al., 2017).

204 Since fast and slow responses are examined from an energetic perspective, we focus on how the atmospheric
205 diabatic cooling (Q) and energy transport terms (H) respond to aerosol perturbations in fSST and MLO
206 simulations. H is calculated offline, as a residual by using the energy budget equation. Following previous studies
207 (e.g., Muller and O'Gorman, 2011; Richardson et al., 2016), Q is the combination of atmospheric radiative cooling
208 (ARC) and downward surface sensible flux (-SH), as follows:

209 $$Q = ARC - SH \tag{3}$$

210 ARC is defined as net shortwave (SW) and longwave (LW) radiation loss of the atmospheric column, which can
211 be calculated from the difference between the top of atmosphere (TOA) and surface radiative fluxes (downward
212 positive), defined as

213 $$ARC = (LW_{TOA} + SW_{TOA}) - (LW_{SUR} + SW_{SUR}) \tag{4}$$

214 Ghan (2013) suggested using additional diagnostics to distinguish aerosol radiative forcing from aerosols, clouds,
215 and surface albedo. This has been widely adopted in current GCMs to better estimate aerosol effects (e.g., Zhang
216 et al., 2016). Following Ghan (2013), we further decompose ARC into contributions from clouds, aerosols and
217 clear-clean sky (without aerosols and clouds) separately (Equation 5), by using the same additional radiation call
218 to calculate ARC from the clear-clean sky ($ARC_{clear,clean}$):

219 $$ARC = ARC_{aerosol} + ARC_{cloud} + ARC_{clear,clean} \tag{5}$$

220 $$ARC_{aerosol} = ARC - ARC_{clean} \tag{6}$$

221 $$ARC_{cloud} = ARC_{clean} - ARC_{clear,clean} \tag{7}$$

222 Since ARC consists of radiative heating/cooling from aerosols (mainly through aerosol direct SW absorption),
223 clouds (primarily through cloud LW absorption/cooling), and clear-clean sky (mainly though LW radiative
224 absorption/cooling from GHGs, water vapour, and Planck feedback), it is helpful to systematically study the effect
225 of absorbing and non-absorbing aerosols on each decomposed energy term, and to further connect those to changes
226 in precipitation.

227 It is worth noting that $\Delta ARC_{aerosol}$ only includes direct interactions with radiation here and is much more sensitive
228 to absorbing aerosol burden rather than non-absorbing aerosols. Despite the significant negative radiative forcing
229 at TOA (Boucher et al., 2013), non-absorbing aerosols do not significantly modify atmospheric radiative
230 absorption, as they act to decrease net SW radiative fluxes at both the surface and TOA in the same way. Non-
231 absorbing aerosols can affect atmospheric radiative absorption via changing absorbing aerosol life cycles (Stier
232 et al., 2006), but the impacts can be very small. It should also be noted here that changes in ARC_{cloud} include
233 aerosol indirect effects (interactions with clouds) on ARC and cloud feedbacks in slow responses, but most of the
234 changes are from LW radiation from clouds (e.g., Lubin and Vogelman, 2006) rather than SW radiation. And its
235 magnitude depends on the temperature (height) at both cloud top and bottom as well as on the ice concentration
236 at cloud top (see Figure S2 for baseline ARC_{cloud}). As aerosol effects on convective clouds are not explicitly
237 simulated in ECHAM6-HAM2 (or most GCMs) yet, changes of ARC_{cloud} from convective clouds are mostly
238 caused by aerosol-induced changes in dynamics. Baseline $\Delta ARC_{aerosol}$, ΔARC_{cloud}, and $\Delta ARC_{clear,clean}$ can be
239 seen in supplementary file (Figure S2, S3, S4).

3. Results

3.1. Global mean responses

242 Table 1 shows the global-mean fast, slow, and total responses of the energy budget terms, including atmospheric
243 latent heat release from precipitation ($L\Delta P$) and other atmospheric diabatic cooling terms, in response to increased
244 BC and SUL emission for the fSST and MLO simulations, respectively. Globally averaged precipitation is
245 decreased in both the BC and SUL experiment, and the associated reduced latent heating is primarily balanced by
246 decreased ARC (Table 1). However, there are some substantial differences between BC and SUL cases after
247 decomposition into different contributions.

248 For the BC case, the decreased precipitation from total responses ($L\Delta P$ around -3.26 W m^{-2}) is mostly contributed
249 by fast responses ($L\Delta P$ around -3.64 W m^{-2}). Slow responses ($L\Delta P$ around 0.38 W m^{-2}) lead to increased but much
250 smaller in magnitude precipitation changes compared to the fast responses. Previous studies suggest that fast
251 responses are largely mediated by atmospheric radiative absorption while slow responses scale with surface
252 temperature change (Samset et al., 2016). An increase of BC emissions can increase atmospheric absorption to a
253 large extent, which is a near-instantaneous process. This can be seen from the decomposition of ARC, which
254 shows that the decreased ARC from fast and total responses is mainly due to the increased SW absorption from
255 BC aerosols ($\Delta ARC_{aerosol}$) (Table 1). However, the change of global-mean surface temperature in the BC case is
256 small (around 0.4 K). That is because for an increase of BC emissions, reduction of downward SW radiation
257 largely counteracts increased downward LW radiation from the warmer atmosphere. As a result, the change of
258 surface temperature is regionally-dependent and globally small (Stjern et al., 2017) (Figure S2). Large changes in
259 $\Delta ARC_{aerosol}$ and small changes in global-mean surface temperature lead to a dominating contribution from fast
260 responses to total global-mean rainfall changes for the BC cases.

261 For the SUL case, the slow response dominates the total response (Table 1). Since SUL is a non-absorbing aerosol,
262 which decreases net SW radiative fluxes at both the surface and TOA through scattering solar radiation,
263 atmospheric absorption changes little. Most of the reduced ARC in the total response is from changes in clear-
264 clean sky radiative cooling ($\Delta ARC_{clear,clean}$) from slow responses mediated via surface flux changes. As SUL

7

265 decreases SW radiation reaching the surface, the global-mean temperature decreases around 2K on a relatively
266 long timescale due to the high capacity of oceans (a slow process). Decreased global-mean temperature further
267 leads to reduced $ARC_{clear,clean}$ from decreased atmospheric column temperature (i.e. Planck feedback) (Zelinka
268 et al., 2020), and decreased water vapour content, which is controlled by the Clausius-Clapyron relationship
269 (Suzuki and Takemura, 2019).
270 The contribution of changes from SH acts to counteract nearly one-third the decreased ARC in fast and total
271 responses for the BC case, which is much larger than that in the SUL case. This is because the absorbing aerosols
272 heat the atmosphere and decrease the temperature difference between near-surface air and the surface, resulting
273 in reduced upward SH fluxes. So changes in SH are also dominated by the fast response, and mainly act to increase
274 precipitation from an energetic perspective, counteracting the decreasing effect induced by ARC in the BC case
275 (Ming et al., 2010).

276 **3.2. Regional responses and their contributions**

277 The geographical patterns of precipitation responses are substantially different between BC and SUL, in both the
278 fast and total responses (Figure 1). The patterns are similar to Samset et al., 2016, in which they showed an
279 ensemble result with a focus on inter-comparison among several models and climate forcers. For the total response,
280 it shows a distinct pattern of an ITCZ shift in response to increased BC and SUL emission. ITCZ tends to shift
281 northward in the BC case while southward in SUL case (Figure 1a and 1b). Since BC warms (SUL cools) the
282 northern hemisphere, there is an enhanced southward (northward) cross-equatorial energy flux in responses to the
283 aerosol perturbation, resulting in ITCZ being shifted towards the warmer hemisphere (Bischoff and Schneider,
284 2016; Wang, 2009). Changes in tropical rainfall are dominated by changes in the Hadley cell in responses to the
285 enhanced cross-hemispheric energy fluxes. Figure 1e and 1f further show that slow response mainly contributes
286 to the ITCZ shift in both cases. This will be further demonstrated in Section 3.3 and 3.4.
287 The fast response of precipitation in the BC case (Figure 1c) shows a land-sea contrast pattern in the tropics, in
288 which rainfall increases in central Africa while it decreases in the surrounding tropical ocean. Central Africa is
289 one of the main source regions of BC emission through biomass burning, and tenfold increase of BC emissions
290 makes the burden changes significant (Figure S1). The pattern of the fast precipitation response in the BC case is
291 similar to the pattern of rapid precipitation response to CO_2 shown in Richardson et al., (2016). But the mechanism
292 is not exactly the same. In the CO_2 case, even though SST remains unchanged, CO_2 can increase land surface
293 temperature and the land-sea temperature contrast (warmer land and unchanged ocean) leads to a shift of
294 convection to over land (Richardson et al., 2016). For an increase of BC emissions, increased downward LW
295 radiation from the warmer atmosphere is largely counteracted by a reduction of downward SW radiation. As a
296 result, surface temperature is decreased in central Africa (Figure S2), which differs from the CO_2 case. But
297 increased BC emission can still warm up the lower troposphere and lead to more ascending motions over Central
298 Africa (Figure S3) (Dagan et al., 2019b; Roeckner et al., 2006). As for the SUL case, the rapid precipitation
299 response shows an opposite land-sea contrast pattern in the tropics, because SUL cools the land temperature
300 (Figure 1d) as land surface temperature is not constrained in fSST runs. However, considering SUL does not
301 directly affect the diabatic heating/cooling in the atmosphere, which differs from BC, the changes are small and
302 not statistically significant over most regions. There are still some exceptions. For example, southeast Asia, which
303 has the largest contribution to SUL emission, and SUL impacts on rainfall through cooling of land temperature as

304 well as interactions with monsoon (e.g., Wang et al., 2019). Decreased surface temperature over continents, such

305 as South America, leads to a decrease of precipitation in most land regions as well as an increase in surrounding

306 oceans (i.e. southeast Pacific Ocean). (Figure 1d).

307 In the zonal-mean, precipitation is decreased over northern hemispheric mid-latitudes in both BC and SUL cases

308 for total responses, but different processes contribute to the total response. Most of the precipitation changes over

309 high latitudes are contributed by fast responses in the BC case (Figure 1g) and slow responses in the SUL case

310 (Figure 1h). Dagan et al., (2019b) showed different responses of rainfall to aerosol perturbation in the tropics and

311 extra-tropics. They demonstrated that precipitation responses are more correlated with the energy transport term

312 (H) in the tropics where heating anomalies can be compensated for by large-scale thermally-driven circulations,

313 whereas extra-tropical rainfall responses are constrained by radiative cooling in the extra-tropics due to the

314 stronger Coriolis force (thus weak energy transport). The different contribution from fast and slow processes

315 between the BC and SUL case indicates different responses in the diabatic cooling in the extra-tropics, and this

316 will be addressed in Figure 3 and Figure 4 from an energetic perspective.

317 Figure 2 quantifies how fast and slow responses contribute to total responses of precipitation on regional scales.

318 We used the response ratio which has also been used in Samset et al., (2016), as follows

319 $R_{resp} = (|\Delta P_{fast}| - |\Delta P_{slow}|)/(|\Delta P_{fast}| + |\Delta P_{slow}|)$ (8)

320 If R_{resp} is larger than 0 and close to 1, it means most of the total responses are contributed by fast responses. If

321 R_{resp} is less than 0 and close to -1, it means slow responses dominates over fast responses. Samset et al., (2016)

322 showed continental-based results of R_{resp} for different climate forcers, and found the variabilities among models.

323 Here Figure 2 focuses only on BC and SUL perturbations, and quantitatively gives us the geographical patterns

324 of contributions from fast and slow responses to total precipitation change. For the BC case, generally the response

325 over northern hemispheric midlatitudes is consistent with the globally averaged result shown in Table 1, in which

326 shows that the precipitation change is dominated by fast responses (Figure 2a). It can be seen from Figure 2a that

327 significant contribution from fast response over North America, northern Atlantic Ocean, Europe, most regions

328 in China, and north-eastern Pacifica Ocean. However, as for the changes in tropical rainfall, which is associated

329 with ITCZ shift seen in the total response, slow responses mainly contribute to the northward shift of ITCZ rather

330 than fast responses in the BC case. One exception is the Central Africa, where the precipitation changes are still

331 dominated by fast responses, and this will be further examined later. For the SUL case, it has been shown that

332 total responses are dominated by slow responses, both globally and regionally (Figure 2b). Some exceptions are

333 some land regions such as America, China and Sahel regions, where the precipitation change is mostly not

334 significant in total responses.

335 **3.3. Changes in energy budget terms**

336 To explain the different mechanisms between BC and SUL in terms of the contribution from fast and slow

337 responses in more detail, we examine the changes in each energy budget term from Equation 1.

338 For the BC case, in fast responses, most decreases in Q are located over the main BC source regions such as

339 Central Africa, Northeast China (Figure 3a and Figure S1). For zonal mean results, after decomposing δQ into

340 different terms based on Equation 3 and 5, it shows aerosol SW absorption is the major contributor to changes in

341 Q (Figure 5a). Since BC is a strongly absorbing aerosol, and the effect is near-instantaneous, the changes of Q

342 lead to decreased precipitation on global and zonal-mean scales and happen through fast responses (Table 1 and

343   Figure 5a). The zonal mean plot (Figure 3e) shows that fast responses of δQ caused by aerosol absorption (Figure

344   5a) leads to reduced rainfall, especially over northern hemispheric midlatitudes (red solid line in Figure 3e).

345   However, on regional scales, the energy transport term acts to play an important role. The geographical pattern of

346   fast precipitation changes (Figure 1c) is more similar to fast response of δH (Figure 3c) (spatial correlation ~0.9)

347   than δQ (spatial correlation ~-0.5). The spatial pattern of fast δH (Figure 3c) also shows a land sea contrast in the

348   tropics as in the precipitation change distribution (Figure 1c), and this is most prominent in Central Africa and

349   middle Atlantic Ocean. There is a significant increase of rainfall over Central Africa and decrease over the middle

350   Atlantic Ocean (Figure 1a). This is mostly contributed by fast responses (Figure 1c and Figure 2a). As mentioned,

351   this pattern is similar to the case of CO_2 shown in Richardson et al., (2016). Although BC decreased surface

352   temperature in Central Africa through fast responses (Figure S2), BC can still warm up the lower troposphere at

353   central Africa, which results in a thermal driven circulation which favours more convections there. This is

354   evidenced by Figure 3c which shows the dry static energy flux flow from Central Africa to the middle Atlantic

355   Ocean (Figure 3c). Dagan et al., (2019b) performed an idealised experiment by adding an absorbing plume in the

356   tropics, and found a very similar standing wave pattern of precipitation as a response. Examining δH shows that

357   this is caused by a thermal driven circulation, which favours more convections over central Africa. Positive δH is

358   consistent with more ascending motions at central Africa (Figure S3). BC warms up the lower troposphere at

359   central Africa, which results in more ascending motions (Figure S3), and the dry static energy flux flow from

360   Central Africa to the middle Atlantic Ocean (Figure 3c).

361   The slow response of δQ leads to a global increase of precipitation (Figure 3b), but the magnitude is an order of

362   magnitude less than the fast response in δQ. This increased precipitation in the slow-response is caused by the

363   associated increase global temperature (Figure 6c) (Table 1). From an energetic perspective, it is mainly associated

364   with the clear-clean sky LW cooling (ARC$_{clear,clean}$) (Table 1 and Figure 5b) as a result of increased atmospheric

365   column temperature (Planck feedback). As precipitation responses in the extra-tropics are more correlated with

366   δQ , larger fast responses of Q explain why rainfall responses in extra-tropics are dominated by the fast response

367   in the BC case (Figure 2a). Figure 3e shows that the ITCZ shift seen in total responses is strongly correlated with

368   slow responses of δH. Warmer northern hemisphere caused by an increase in BC leads to a southward cross-

369   equatorial energy flux, which is accompanied by a northward shift of Hadley cell (Bischoff and Schneider, 2016).

370   Changes in vertical pressure velocity can be found in Figure 6, which also indicates a northward shift of the

371   ascending branch of the Hadley cell. From an energetic view, the changes in vertical pressure velocity drive the

372   dynamic effect on advection of dry static energy, which is a strong component in the changes of divergence of

373   dry static energy fluxes (δH) in the tropics (Richardson et al., 2016).

374   For the SUL case, most of the fast responses are not statistically significant (Figure 4a and 4c), and total responses

375   are dominated by the slow response. For changes in extra-tropics, changes in Q are correlated with changes in

376   precipitation. SUL decreases the mean-state temperature of troposphere through slow responses, which leads to a

377   reduction of specific humidity (Figure 7). From an energetic view, it leads to a decreased clean-clear sky radiative

378   cooling (ARC$_{clear,clean}$) (Figure 5d), which contributes to most of the reduced slow responses of δQ. For changes

379   in the tropics, like the BC case, slow responses of δH are consistent with the southward ITCZ shift in the total

380   response (Figure 4d). In the extra-tropics, for the SUL case, there is also an interesting land-sea contrast in both

381   fast and slow δH, with dry static energy fluxes generally diverging from oceans to lands in fast δH (Figure 4c)

382   and converging in slow δH (Figure 4d). This is because in the fixed SST simulations, land surface temperature is

still allowed to decrease in response to increased SUL emission (Figure S5b) as a result of reduced downward SW radiation. The land-sea contrast of temperature (colder land) results in more downward large-scale motions and divergence of moisture (See Figure S6 for changes in vertical pressure velocity and column-integrated water vapour) over most land regions, particular Southeast Asia and South America, in fast responses. Since fast responses have already accounted part of land temperature reduction, ocean surface temperature decreases more than land surface in slow responses (Figure S2d). The colder ocean temperature therefore leads to an opposite land-sea pattern compared to fast responses (Figure 4d).

Changes of Q are more robust in the fast response for the BC case, and the slow response of Q is more robust for the SUL case. Decomposition of diabatic cooling shows its global-mean decrease is dominated by an increase of atmospheric aerosol absorption for fast responses in BC case (Figure 5a) and decreased radiative cooling from the clear-clean sky for slow responses in the SUL case (Figure 5d). The decreased $ARC_{clear,clean}$ are mainly caused by the decreased atmospheric column temperature (Planck feedback) and associated reduced water vapour content (controlled by the Clausius-Clapyron relationship). Sensible heat flux (upward) is also reduced due to the warmer atmosphere caused by absorption from BC (Figure 5a).

It should also be noted that changes in diabatic cooling counteract the latent heat released from precipitation associated with the ITCZ shift in both cases (Figure 3b and Figure 4b). This is mainly caused by ARC_{clouds}, as it contributes a large part of diabatic cooling over tropical regions (Figure 5b and 5d). This counteraction with the ITCZ shift is caused by the associated change of deep convective clouds (see supplementary file for changes in cloud properties). This is consistent with the results shown in Naegele and Randall, (2019). They found a negative correlation between tropical rainfall and diabatic cooling and demonstrated this is caused by feedbacks from deep convective clouds. More high clouds lead to a decrease of atmospheric LW radiative cooling but an increase of precipitation, and the negative correlation is robust over tropical regions where deep convective clouds prevail (Naegele and Randall, 2019). The spatial patterns of fast, slow and total responses to $\Delta ARC_{aerosol}$, ΔARC_{cloud}, and $\Delta ARC_{clear,clean}$ can be found in supplementary file.

3.4. Responses of large-scale circulation and local thermodynamic conditions

Figure 3e and Figure 4e show that changes in tropical rainfall are strongly associated with slow responses of the energy transport term, independent of aerosol types (absorbing or non-absorbing), whereas changes in mid-latitude precipitation are dependent on aerosol types, which are dominated by fast responses of aerosol SW absorption in the BC case and slow responses of clear-clean sky radiative cooling in the SUL case. To help understand the mechanisms of the tropospheric response in different regions, we study the response of the large-scale circulation and thermodynamic conditions, by examining the changes in vertical pressure velocity (ω), temperature T, and specific humidity q (Figure 6 and Figure 7). The vertical pressure velocity (ω) at 500hPa is a useful method to distinguish different cloud dynamic regimes, and a metric to quantify the strength of large-scale circulation (Bony and Dufresne, 2005; Zhang et al., 2016). Here we only show zonal mean analysis.

As shown in Figure 6, BC warms up the atmosphere through SW absorption, and the warming is confined mainly in the Northern Hemisphere (NH) where the BC emissions prevail. This leads to southward cross-equatorial energy fluxes and northward shift of the Hadley cell (Wang, 2009; Bischoff and Schneider, 2016; Zhao and Suzuki, 2019). The changes in ω demonstrate the northward shift of the ascending branch of the Hadley cell, which show an increased upward motion in NH tropics and decreased ascending motion in SH tropics (Figure 6d). Therefore,

the tropical rainfall associated with ITCZ changes in response to the changes of large circulation. Figure 6f further demonstrates that slow responses contribute to most of the changes in tropical large-scale circulations in Figure 6d. It is consistent with Figure 3 that changes in tropical latent heat released from precipitation is mostly contributed by $\delta H(\text{slow})$, because the dynamic component associated with changes vertical velocity dominates the energy transport term over tropics (Richardson et al., 2016). Outside the tropics, changes in ω are not as significant as in tropics (Figure 6d), and zonal mean rainfall is more related to local changes in thermodynamic conditions. Absorbing aerosols directly heat the mid-troposphere through fast processes (Figure 6b). Heating the mid-troposphere will stabilise the column and suppress precipitation. This is consistent with the energetic perspective shown in Figure 3 and Figure 5a that fast responses of radiative cooling caused by BC SW absorption (reduced $ARC_{aerosol}$) accounts for the decreased latent heat in extra-tropics. An interesting aspect here is that while BC induces the ITCZ shift, the fast response (Figure 6e) seems to counteract the stronger slow response shown in Figure 6f. This is because of the strong non-zonal effect from Central Africa (see geographical pattern of vertical pressure velocity changes in the supplementary file), where BC warms up the lower troposphere resulting in more ascending motions in fast responses (Figure S6). It is also consistent with Figure 1g that fast responses of rainfall in southern tropical branch act to enhance ITCZ while only northern branch act to decrease ITCZ.

For the SUL case, the tropical rainfall response is opposite to that in the BC case, but the mechanism is similar. Increasing sulphate aerosols induces a dimming effect and causes a negative radiative forcing at the surface, which is as fast process. Subsequently, global surface temperatures are decreased, a slow process controlled by ocean heat capacity, , and this cooling is more significant in NH (Figure 7a and 7c). As a result, the northward cross-equatorial energy fluxes lead to a southward shift of the Hadley cell (Figure 7d). The slow responses of the large-scale circulation (caused by SST temperature difference between hemispheres) contributes most of the shift of Hadley cell (Figure 7e). In the extra-tropics, a decrease of precipitation is also found in response to changes in thermodynamics. However, unlike black carbon, SUL decreases surface temperature through slow processes and leads to a cooling of the whole column in the extra-tropics (Figure 7a and 7c). As a result, the specific humidity shows a large reduction (Figure 7i), which is associated with a reduction of rainfall in the extra-tropics. This is consistent with the energetic perspective shown in Figure 4 and Figure 5d that reduced clean-clear sky radiative cooling ($ARC_{clear,clean}$) accounts for the decreased latent heat in extra-tropics.

It is worth mentioning that Figure 6 and Figure 7, as a bottom-up method, qualitatively show how the changes in large-scale circulation and local thermodynamics affect rainfall in terms of total, fast, and slow responses respectively, whereas the energy budget view (Figure 3, 4, and 5), as a top-down method, is easier to quantify these contributions through energetic terms (e.g., the energy transport term, $ARC_{aerosol}$ and $ARC_{clear,clean}$). Combining these two methods makes the link between precipitation and aerosols explicit.

4. Conclusions

We have examined the response of precipitation to absorbing and non-absorbing aerosol perturbations by separately increasing BC emission and SUL emission in ECHAM6-HAM2 by 10-times and 5-times their baseline emission, following the PDRMIP protocol (Myhre et al., 2017; Samset et al., 2016). The precipitation response is separated into fast (mediated by near-instantaneous changes in atmospheric radiative cooling) and slow responses

460   (mediated by changes in SST) on both global and regional scales. An energetic perspective has been adopted to

461   study precipitation changes. Global-averaged energetics have previously been used to study precipitation

462   responses (e.g., Ming et al., 2010; some PDRMIP work); here, we further decompose atmospheric heating rates

463   into individual terms separately for fast and slow responses. Changes in atmospheric latent heat release from

464   precipitation is balanced by changes in atmospheric radiative cooling (ARC), surface sensible heat flux and local

465   energy transport. We introduce a method, based on Ghan (2013), to further decompose ARC into contributions

466   from aerosols (through aerosol direct SW absorption), clouds (through cloud LW absorption/cooling), and clear-

467   clean sky (without aerosols or clouds; mainly though LW radiative absorption/cooling from GHGs, water vapour,

468   i.e. Planck feedback).

469   While it has long been appreciated that changes in ARC are essential in balancing latent heat released from

470   precipitation on global scales, their relationship on zonal mean or regional scales has not been fully explored. For

471   global means, although SUL and BC have a different sign of radiative forcing at TOA (Boucher et al., 2013), we

472   found that precipitation is decreased for both cases, which is energetically balanced by reduced atmospheric

473   diabatic cooling δQ (Table 1). This response occurs at different timescales, dominated by fast responses for BC

474   and by slow responses for SUL. For BC, on the global scale, the most significant effect is that absorbing aerosols

475   directly heat the mid-troposphere, stabilise the column, and suppress precipitation. Therefore, most of the changes

476   are due to aerosol absorption ($ARC_{aerosol}$) from fast responses. Meanwhile BC warms up the lower troposphere

477   and decrease the temperature differences between the surface and near-surface temperature, which results in a

478   decreased upward sensible heat. Investigating the energy balance, we found this decreased upward surface heat

479   fluxes from fSST experiment acts to cancel almost one third the decreasing effect caused by increased aerosol

480   SW absorption. For SUL, although non-absorbing aerosol does not directly affect ARC through aerosol absorption,

481   the net negative radiative forcing at TOA in fSST experiments and associated surface forcing leads to a decrease

482   of global surface temperature through slow responses. As a result, it cools the whole atmospheric column,

483   accompanied by reduced specific humidity, which leads to reduce precipitation. This can also be seen from the

484   decreased radiative cooling from the clean-clear sky $ARC_{clear,clean}$ in slow responses.

485   Zonally averaged patterns of precipitation changes for the BC and SUL cases are different (Figure 1). Tropical

486   rainfall is primarily associated with ITCZ, which shifts northward for BC, and southward for SUL. Extra-tropical

487   rainfall is reduced in both cases. For BC, slow responses account for most of the changes in tropical rainfall, while

488   fast responses dominate changes in other regions (Figure 2a). BC warms the northern hemisphere through slow

489   responses, which leads to a southward energy flux (Bischoff and Schneider, 2016; Rotstayn and Lohmann, 2002).

490   From an energetic perspective, in the tropics where intense convections and large-scale thermally driven

491   circulations prevail, slow responses of the energy transport term dominate the changes in tropical rainfall (Figure

492   3e), which is associated with the northward shift of Hadley cells (Figure 6). Outside the tropics, BC warms up the

493   mid-troposphere, stabilises the atmosphere (Figure 6) and suppresses precipitation, which is a fast response.

494   Energetically, different from the tropics, BC induced increased diabatic heating is locally confined due to stronger

495   Coriolis force. This geostrophic confinement of the diabatic heating associated with increased aerosols shortwave

496   absorption has to be balanced by reduced latent heat from precipitation (a fast response) (Figure 5a). For the SUL

497   case, the slow response dominates in nearly all regions (Figure 2b), which is not surprising given that sulphate

498   aerosol does not directly affect the column diabatic cooling. In the extra-tropics, SUL decreases surface

499   temperatures, primarily through slow processes, cools the whole column, and reduces specific humidity (Figure

13

7). From an energetic perspective, this can also be seen from the decreased radiative cooling from the clean-clear sky (without clouds and aerosols) (Figure 5d) due to the reduced water vapour content and decreased atmospheric column temperature (Planck feedback).

There exist some interesting regions where the responses are distinct from globally or zonally averaged results. Rainfall is significantly increased over the Central Africa, in the BC case, together with reduced precipitation over the middle Atlantic Ocean, and this pattern is most prominent in fast responses. This pattern shows clear similarities with the standing wave pattern response of precipitation to an idealised plume of absorbing aerosols in the tropics (Dagan et al., 2019b). Examining δH shows that this is caused by a thermally driven circulation, which favours more convections over central Africa. BC warms up the lower troposphere at central Africa, which results in more ascending motions (Figure S3). The low latitude (thus weak Coriolis force) allows for the dry static energy to be efficiently diverged from Central Africa to the middle Atlantic Ocean (Figure 3c). In the SUL case, while most regions are dominated by slow responses, in some regions, such as most parts of China and South America, rainfall changes are still dominated by fast responses (Figure 2b), where the surface temperature is significantly decreased (Figure S2). This is due to the dimming effect from SUL and associated surface flux changes, and because changes of land surface temperature are not constrained in fSST experiments. Reduced surface fluxes and temperatures therefore lead to a decrease of precipitation over most land regions as well as an increase at surrounding oceans (e.g., southeast Pacific Ocean).

Changes in zonally averaged vertical pressure velocity, temperature profile, and specific humidity (Figure 6 and Figure 7) show consistency with zonally averaged energetics. Changes in vertical pressure velocity indicate a northward shift of the ascending branch of the Hadley cell in the BC case and SUL case. It is consistent with the changes in the divergence of dry static energy fluxes, which is dominated by the changes in vertical velocity (the dynamic component) in the tropics (Richardson et al., 2016). In the extra-tropics, stabilisation induced by BC through fast response is consistent with increased atmospheric radiative heating from aerosol SW absorption. Reduced specific humidity as well as decreased atmospheric column temperature in the SUL case is consistent with decreased radiative cooling from the clean-clear sky. The changes in large-scale circulations and local thermodynamics qualitatively explains the responses of precipitation, whereas the energetic perspective provides a method to quantify and make their contributions explicit.

In summary, we examined the relationship between aerosol-induced changes in atmospheric energetics and precipitation changes across different scales. Generally, changes in ARC and latent heat from precipitation are largely balanced on global and extra-tropics (Dagan et al., 2019b). However, these two terms are less balanced in the tropics due to efficient local energy transport. We introduced a new decomposition method, derived from Ghan (2013), to examine aerosol effects on precipitation. For absorbing aerosols, decreased global-mean and extra-tropical precipitation is associated with increased atmospheric aerosol SW absorption from fast responses, while for non-absorbing aerosols, reduced rainfall is more correlated with decreased clear-clean sky atmospheric radiative cooling from slow responses. This top-down method, together with traditional bottom-up method, can make the link between precipitation and aerosols explicit and quantify contributions to global and regional rainfall changes.

We noted that high resolutions are desirable for the analysis of regional precipitation changes. However, climate models in such configurations have been widely used in this context (the entire CMIP and PDRMIP exercises rely on this) and been shown to have skills in examining regional rainfalls as well as their responses (e.g. Liu et al.,

540   2018; Myhre et al., 2017; Samset et al., 2016). Increasing resolution while retaining parameterised convection, as
541   done in many regional climate modelling studies, raises other concerns as many assumptions underlying these
542   parameterisations are no longer valid (Prein et al., 2015). Ultimately, such work should be conducted in cloud
543   resolving configurations (which would also allow to couple aerosols directly to the convection, an effect that is
544   not currently represented) and work is ongoing to develop the required tools. However, it will still be decades
545   before these are routinely available. In the context of the focus of this work, with focus on constraints from the
546   energy budget and the underlying physical constraints in general, GCMs are in fact a very robust tool (and
547   ECHAM6-HAM is, unlike other GCMs or many cloud resolving models, fully energy conserving). We therefore
548   believe our approach to be robust, in-line with a vast body of literature on this very topic (e.g. Jordan et al., 2018;
549   Myhre et al., 2017; Roeckner et al., 2006; Samset et al., 2016; Shawki et al., 2018; Samset et al., 2016). We also
550   note that internal variability on regional scales is significant, in particular in coupled simulations. However, since
551   we are examining the average of last fifty years results instead of the transient evolution, the impacts from internal
552   variability should be small in this case. Therefore, this does not take away from our analysis of physical constraints
553   on precipitation changes.

554   This metric provides further insights into the model variability in simulating rainfall and their responses to
555   different climate forcers, as shown by some PDRMIP research (e.g., Richardson et al., 2018; Stjern et al., 2018).
556   For example, it has been demonstrated that the response from BC perturbation contributes to a large part of the
557   substantial uncertainties among GCMs in simulating the changes in surface temperature and therefore
558   precipitation (Stjern et al., 2017). Distinguishing contributions from individual energetic terms is helpful to assess
559   uncertainties from aerosol absorption, or feedbacks from clouds, water vapour and surface sensible heat flux. This
560   will improve our understanding of GCMs and the climate system, which will be the focus of our follow-up work.
561   There exist some caveats when considering real-world implications of our results. The aerosol perturbation
562   follows the PDRMIP protocol designed to reveal the fundamental mechanisms and to make the aerosol effect
563   strong enough to be distinguishable from natural variability. However, these perturbations are too large to be
564   representative for real-world situations, in particular considering anthropogenic SO_2 (the precursor of SUL)
565   emissions that are starting to decrease in South-east Asia (Zheng et al., 2018). As for Northern Hemispheric
566   midlatitudes, where the population is concentrated, results here show that increased BC or SUL will lead to
567   decreased precipitation, but this happens at different time scales. Increased BC may lead to a near-instantaneous
568   decreased precipitation over China or America, while increased SUL will reduce precipitation via the slow
569   response, modulated by SSTs, at a much longer time scale. In the real world, it should be mentioned that the
570   anthropogenic emissions create a mixture of absorbing and non-absorbing aerosols, so the changes in rainfall
571   strongly depend on the time scale and the real-world emission scenario. It should also be noted that the total
572   responses of precipitation in this work are derived from mixed-layer ocean experiments and therefore differ from
573   real-world changes involving changes in the ocean circulation. There are several studies that have addressed the
574   importance of using ocean-coupled models to accurately simulates regional and global precipitation responses
575   (e.g., Wang et al., 2017; Zhao and Suzuki, 2019).

576

577   **Data availability:** The datasets of original simulations are from the ARCHER facility upon request. The data
578   used to present in this paper can be found at: http://dx.doi.org/10.17632/8n2vj578r2.1 (Zhang, 2021)

579

593

References

594

Ackerman, A. S., Kirkpatrick, M. P., Stevens, D. E. and Toon, O. B.: The impact of humidity above stratiform clouds on indirect aerosol climate forcing, Nature, 432(7020), 1014–1017, doi:10.1038/nature03174, 2004.

595
596

Alizadeh-Choobari, O.: Impact of aerosol number concentration on precipitation under different precipitation rates, Meteorol. Appl., 25(4), 596–605, doi:10.1002/met.1724, 2018.

597
598

Abdul-Razzak, H. and Ghan, S. J.: A parameterization of aerosol activation: 2. Multiple aerosol types, J. Geophys. Res. Atmos., 105(D5), 6837–6844, doi:10.1029/1999JD901161, 2000.

599
600

Allen, M. R. and Ingram, W. J.: Constraints on future changes in climate and the hydrologic cycle, Nature, 419(6903), doi:10.1038/nature01092, 2002.

601
602

Andrews, T., Forster, P. M. and Gregory, J. M.: A surface energy perspective on climate change, J. Clim., 22(10), 2557–2570, doi:10.1175/2008JCLI2759.1, 2009.

603
604

Andrews, T., Forster, P. M., Boucher, O., Bellouin, N. and Jones, A.: Precipitation, radiative forcing and global temperature change, Geophys. Res. Lett., 37(14), doi:10.1029/2010GL043991, 2010.

605
606

Bai, H., Gong, C., Wang, M., Zhang, Z. and L'Ecuyer, T.: Estimating precipitation susceptibility in warm marine clouds using multi-sensor aerosol and cloud products from A-Train satellites, Atmos. Chem. Phys., 18(3), 1763–1783, doi:10.5194/acp-18-1763-2018, 2018.

607
608
609

Bala, G., Caldeira, K. and Nemani, R.: Fast versus slow response in climate change: Implications for the global hydrological cycle, Clim. Dyn., 35(2), 423–434, doi:10.1007/s00382-009-0583-y, 2010.

610
611

Bischoff, T. and Schneider, T.: The equatorial energy balance, ITCZ position, and double-ITCZ bifurcations, J. Clim., 29(8), 2997–3013, doi:10.1175/JCLI-D-15-0328.1, 2016.

612
613

Bony, S. and Dufresne, J. L.: Marine boundary layer clouds at the heart of tropical cloud feedback uncertainties in climate models, Geophys. Res. Lett., 32(20), 1–4, doi:10.1029/2005GL023851, 2005.

614
615

Bony, S., Bellon, G., Klocke, D., Sherwood, S. and Fermepin, S.: Robust direct effect of carbon dioxide on tropical circulation and regional precipitation, Nat. Geosci., 6(6), 447–451, doi:10.1038/ngeo1799, 2013.

616
617

Boucher, O., Randall, D., Artaxo, P., Bretherton, C., Feingold, G., Forster, P., Kerminen, V.-M. V.-M., Kondo, Y., Liao, H., Lohmann, U., Rasch, P., Satheesh, S. K., Sherwood, S., Stevens, B., Zhang, X. Y. and Zhan, X. Y.: Clouds and Aerosols, Clim. Chang. 2013 Phys. Sci. Basis. Contrib. Work. Gr. I to Fifth Assess. Rep. Intergov. Panel Clim. Chang., 571–657, doi:10.1017/CBO9781107415324.016, 2013.

618
619
620
621

Chemke, R. and Dagan, G.: The effects of the spatial distribution of direct anthropogenic aerosols radiative forcing on atmospheric circulation, J. Clim., 31(17), 7129–7145, doi:10.1175/JCLI-D-17-0694.1, 2018.

622
623

624   Dagan, G., Stier, P. and Watson-Parris, D.: Analysis of the Atmospheric Water Budget for Elucidating the Spatial
625   Scale of Precipitation Changes Under Climate Change, Geophys. Res. Lett., 46(17–18), 10504–10511,
626   doi:10.1029/2019GL084173, 2019a.

627   Dagan, G., Stier, P. and Watson-Parris, D.: Contrasting Response of Precipitation to Aerosol Perturbation in the
628   Tropics and Extratropics Explained by Energy Budget Considerations, Geophys. Res. Lett., 46(13), 7828–7837,
629   doi:10.1029/2019GL083479, 2019b.

630   Dallafior, T. N., Folini, D., Knutti, R. and Wild, M.: Mixed-layer ocean responses to anthropogenic aerosol
631   dimming from 1870 to 2000, J. Geophys. Res. Atmos., 121(1), 49–66, doi:10.1002/2015JD024070, 2016.

632   DeAngelis, A. M., Qu, X., Zelinka, M. D. and Hall, A.: An observational radiative constraint on hydrologic cycle
633   intensification, Nature, 528(7581), 249–253, doi:10.1038/nature15770, 2015.

634   Dentener, F., Kinne, S., Bond, T., Boucher, O., Cofala, J., Generoso, S., Ginoux, P., Gong, S., Hoelzemann, J. J.,
635   Ito, A., Marelli, L., Penner, J. E., Putaud, J.-P., Textor, C., Schulz, M., van der Werf, G. R. and Wilson, J.:
636   Emissions of primary aerosol and precursor gases in the years 2000 and 1750 prescribed data-sets for AeroCom,
637   Atmos. Chem. Phys., 6(12), 4321–4344, doi:10.5194/acp-6-4321-2006, 2006.

638   Forster, P., Ramaswamy, V., Artaxo, P., Berntsen, T., Betta, R., Fahey, D. W., Haywood, J., Lean, J., Lowe, D.
639   C., Myhre, G., Nganga, J., Prinn, R., Raga, G., Schulz, M., and Van Dorland, R.: Changes in atmospheric
640   constituents and in radiative forcing, in Climate Change 2007: The Physical Science Basis. Contribution of
641   Working Group I to the Fourth Assessment Report of the Intergovernmental Panel on Climate Change, edited by:
642   Solomon, S., Qin, D., Manning, M., Chen, Z., Marquis, M., Averyt, K. B., Tignor, M., and Miller, H. L.,
643   Cambridge University Press, New York, NY, 2007.

644   Gettelman, A., Morrison, H., Terai, C. R. and Wood, R.: Microphysical process rates and global aerosol-cloud
645   interactions, Atmos. Chem. Phys., 13(19), 9855–9867, doi:10.5194/acp-13-9855-2013, 2013.

646   Ghan, S., Wang, M., Zhang, S., Ferrachat, S., Gettelman, A., Griesfeller, J., Kipling, Z., Lohmann, U., Morrison,
647   H., Neubauer, D., Partridge, D. G., Stier, P., Takemura, T., Wang, H. and Zhang, K.: Challenges in constraining
648   anthropogenic aerosol effects on cloud radiative forcing using present-day spatiotemporal variability, Proc. Natl.
649   Acad. Sci., 113(21), 5804–5811, doi:10.1073/pnas.1514036113, 2016.

650   Ghan, S. J.: Technical Note: Estimating aerosol effects on cloud radiative forcing, Atmos. Chem. Phys., 13(19),
651   9971–9974, doi:10.5194/acp-13-9971-2013, 2013.

652   Ghan, S. J., Liu, X., Easter, R. C., Zaveri, R., Rasch, P. J., Yoon, J. H. and Eaton, B.: Toward a minimal
653   representation of aerosols in climate models: Comparative decomposition of aerosol direct, semidirect, and
654   indirect radiative forcing, J. Clim., 25(19), 6461–6476, doi:10.1175/JCLI-D-11-00650.1, 2012.

655   Gregory, J. and Webb, M.: Tropospheric Adjustment Induces a Cloud Component in CO2 Forcing, J. Clim., 21(1),
656   58–71, doi:10.1175/2007JCLI1834.1, 2008.

657   Gryspeerdt, E., Stier, P. and Partridge, D. G.: Links between satellite-retrieved aerosol and precipitation, Atmos.

658   Chem. Phys., 14(18), 9677–9694, doi:10.5194/acp-14-9677-2014, 2014.

659   Haynes, J. M., L'Ecuyer, T. S., Stephens, G. L., Miller, S. D., Mitrescu, C., Wood, N. B. and Tanelli, S.: Rainfall

660   retrieval over the ocean with spaceborne W-band radar, J. Geophys. Res. Atmos., 114(8), 1–18,

661   doi:10.1029/2008JD009973, 2009.

662   Johnson, B. T., Haywood, J. M. and Hawcroft, M. K.: Are Changes in Atmospheric Circulation Important for

663   Black Carbon Aerosol Impacts on Clouds, Precipitation, and Radiation?, J. Geophys. Res. Atmos., 124(14), 7930–

664   7950, doi:10.1029/2019jd030568, 2019.

665   Jordan, A. K., Gnanadesikan, A. and Zaitchik, B.: Simulated Dust Aerosol Impacts on Western Sahelian Rainfall:

666   Importance of Ocean Coupling, J. Clim., 31(22), 9107–9124, doi:10.1175/JCLI-D-17-0819.1, 2018.

667   Kasoar, M., Shawki, D. and Voulgarakis, A.: Similar spatial patterns of global climate response to aerosols from

668   different regions, npj Clim. Atmos. Sci., 1(1), 12, doi:10.1038/s41612-018-0022-z, 2018.Khairoutdinov, M. and

669   Kogan, Y.: A New Cloud Physics Parameterization in a Large-Eddy Simulation Model of Marine Stratocumulus,

670   Mon. Weather Rev., 128(1), 229–243, doi:10.1175/1520-0493(2000)128<0229:ANCPPI>2.0.CO;2, 2000.

671   Keshtgar, B., Alizadeh-Choobari, O. and Irannejad, P.: Seasonal and interannual variations of the intertropical

672   convergence zone over the Indian Ocean based on an energetic perspective, Clim. Dyn., 54(7–8), 3627–3639,

673   doi:10.1007/s00382-020-05195-5, 2020.

674   Khain, A. P.: Notes on state-of-the-art investigations of aerosol effects on precipitation: a critical review, Environ.

675   Res. Lett., 4(1), 015004, doi:10.1088/1748-9326/4/1/015004, 2009.

676   Khain, A. P., BenMoshe, N. and Pokrovsky, A.: Factors Determining the Impact of Aerosols on Surface

677   Precipitation from Clouds: An Attempt at Classification, J. Atmos. Sci., 65(6), 1721–1748,

678   doi:10.1175/2007JAS2515.1, 2008.

679   Köhler, H.: The nucleus in and the growth of hygroscopic droplets, Trans. Faraday Soc.,

680   doi:10.1039/TF9363201152, 1936.

681   Kvalevåg, M. M., Samset, B. H. and Myhre, G.: Hydrological sensitivity to greenhouse gases and aerosols in a

682   global climate model, Geophys. Res. Lett., 40(7), 1432–1438, doi:10.1002/grl.50318, 2013.

683   Lamarque, J.-F., Bond, T. C., Eyring, V., Granier, C., Heil, A., Klimont, Z., Lee, D., Liousse, C., Mieville, A.,

684   Owen, B., Schultz, M. G., Shindell, D., Smith, S. J., Stehfest, E., Van Aardenne, J., Cooper, O. R., Kainuma, M.,

685   Mahowald, N., McConnell, J. R., Naik, V., Riahi, K. and van Vuuren, D. P.: Historical (1850–2000) gridded

686   anthropogenic and biomass burning emissions of reactive gases and aerosols: methodology and application,

687   Atmos. Chem. Phys., 10(15), 7017–7039, doi:10.5194/acp-10-7017-2010, 2010.

688   Lambert, F. H. and Webb, M. J.: Dependency of global mean precipitation on surface temperature, Geophys. Res.

689   Lett., 35(16), 1–5, doi:10.1029/2008GL034838, 2008.

690   Lebo, Z. J. and Feingold, G.: On the relationship between responses in cloud water and precipitation to changes
691   in aerosol, Atmos. Chem. Phys., 14(21), 11817–11831, doi:10.5194/acp-14-11817-2014, 2014.

692   Liu, L., Shawki, D., Voulgarakis, A., Kasoar, M., Samset, B. H., Myhre, G., Forster, P. M., Hodnebrog, Sillmann,
693   J., Aalbergsjø, S. G., Boucher, O., Faluvegi, G., Iversen, T., Kirkevåg, A., Lamarque, J. F., Olivié, D., Richardson,
694   T., Shindell, D. and Takemura, T.: A PDRMIP Multimodel study on the impacts of regional aerosol forcings on
695   global and regional precipitation, J. Clim., 31(11), 4429–4447, doi:10.1175/JCLI-D-17-0439.1, 2018.

696   Liu, Z., Wang, M., Rosenfeld, D., Zhu, Y., Bai, H., Cao, Y. and Liang, Y.: Evaluation of Cloud and Precipitation
697   Response to Aerosols in WRF-Chem With Satellite Observations, J. Geophys. Res. Atmos., 125(18), 1–25,
698   doi:10.1029/2020JD033108, 2020.

699   Lohmann, U. and Hoose, C.: Sensitivity studies of different aerosol indirect effects in mixed-phase clouds, Atmos.
700   Chem. Phys., 9(22), 8917–8934, doi:10.5194/acp-9-8917-2009, 2009.

701   Lohmann, U., Stier, P., Hoose, C., Ferrachat, S., Kloster, S., Roeckner, E. and Zhang, J.: Cloud microphysics and
702   aerosol indirect effects in the global climate model ECHAM5-HAM, Atmos. Chem. Phys., 7(13), 3425–3446,
703   doi:10.5194/acp-7-3425-2007, 2007.

704   Lubin, D. and Vogelmann, A. M.: A climatologically significant aerosol longwave indirect effect in the Arctic,
705   Nature, 439(7075), 453–456, doi:10.1038/nature04449, 2006.

706   Michibata, T., Suzuki, K., Sato, Y. and Takemura, T.: The source of discrepancies in aerosol–cloud–precipitation
707   interactions between GCM and A-Train retrievals, Atmos. Chem. Phys., 16(23), 15413–15424, doi:10.5194/acp-
708   16-15413-2016, 2016.

709   Ming, Y., Ramaswamy, V. and Persad, G.: Two opposing effects of absorbing aerosols on global-mean
710   precipitation, Geophys. Res. Lett., 37(13), 1–4, doi:10.1029/2010GL042895, 2010.

711   Muller, C. J. and O'Gorman, P. A.: An energetic perspective on the regional response of precipitation to climate
712   change, Nat. Clim. Chang., 1(5), 266–271, doi:10.1038/nclimate1169, 2011.

713   Myhre, G., Forster, P. M., Samsmset, B. H., Odnebrog, Sillmann, J., Aalbergsjø, S. G., Andrews, T., Boucher, O.,
714   Faluvegi, G., Fläschner, D., Iversen, T., Kasoar, M., Kharin, V., Kirkevag, A., Lamarque, J. F., Olivié, D.,
715   Richardson, T. B., Shindell, D., Shine, K. P., Stjern, C. W., Takemura, T., Voulgarakis, A. and Zwiers, F.:
716   PDRMIP: A precipitation driver and response model intercomparison project-protocol and preliminary results,
717   Bull. Am. Meteorol. Soc., 98(6), 1185–1198, doi:10.1175/BAMS-D-16-0019.1, 2017.

718   Naegele, A. C. and Randall, D. A.: Geographical and Seasonal Variability of Cloud-Radiative Feedbacks on
719   Precipitation, J. Geophys. Res. Atmos., 124(2), 684–699, doi:10.1029/2018JD029186, 2019.

720   Neubauer, D., Ferrachat, S., Siegenthaler-Le Drian, C., Stier, P., Partridge, D. G., Tegen, I., Bey, I., Stanelle, T.,
721   Kokkola, H. and Lohmann, U.: The global aerosol–climate model ECHAM6.3–HAM2.3 – Part 2: Cloud
722   evaluation, aerosol radiative forcing, and climate sensitivity, Geosci. Model Dev., 12(8), 3609–3639,
723   doi:10.5194/gmd-12-3609-2019, 2019.

724   Nordeng, T. E.: Extended versions of the convective parametrization scheme at ECMWF and their impact on the
725   mean and transient activity of the model in the tropics, ECMWF Research Department, Technical Momorandum
726   206, European Centre for Medium-range Weather Forecast, Reading, UK, 1994.

727   O'Gorman, P. A., Allan, R. P., Byrne, M. P. and Previdi, M.: Energetic Constraints on Precipitation Under Climate
728   Change, Surv. Geophys., 33(3–4), 585–608, doi:10.1007/s10712-011-9159-6, 2012.

729   Pendergrass, A. G. and Hartmann, D. L.: Global-mean precipitation and black carbon in AR4 simulations,
730   Geophys. Res. Lett., 39(1), 1–6, doi:10.1029/2011GL050067, 2012.

731   Pincus, R. and Stevens, B.: Paths to accuracy for radiation parameterizations in atmospheric models, J. Adv.
732   Model. Earth Syst., 5(2), 225–233, doi:10.1002/jame.20027, 2013.

733   Prein, A. F., Langhans, W., Fosser, G., Ferrone, A., Ban, N., Goergen, K., Keller, M., Tölle, M., Gutjahr, O.,
734   Feser, F., Brisson, E., Kollet, S., Schmidli, J., Lipzig, N. P. M. and Leung, R.: A review on regional convection-
735   permitting climate modeling: Demonstrations, prospects, and challenges, Rev. Geophys., 53(2), 323–361,
736   doi:10.1002/2014RG000475, 2015.

737   Ramanathan, V., Crutzen, P. J., Kiehl, J. T. and Rosenfeld, D: Aerosols, Climate, and the Hydrological Cycle,
738   Science (80-.)., 294(5549), 2119–2124, doi:10.1126/science.1064034, 2001.

739   Richardson, T. B., Forster, P. M., Andrews, T. and Parker, D. J.: Understanding the rapid precipitation response
740   to CO2 and aerosol forcing on a regional scale, J. Clim., 29(2), 583–594, doi:10.1175/JCLI-D-15-0174.1, 2016.

741   Richardson, T. B., Forster, P. M., Andrews, T., Boucher, O., Faluvegi, G., Fläschner, D., Hodnebrog, Ø., Kasoar,
742   M., Kirkevåg, A., Lamarque, J.-F., Myhre, G., Olivié, D., Samset, B. H., Shawki, D., Shindell, D., Takemura, T.
743   and Voulgarakis, A.: Drivers of Precipitation Change: An Energetic Understanding, J. Clim., 31(23), 9641–9657,
744   doi:10.1175/JCLI-D-17-0240.1, 2018.

745   Roeckner, E., Stier, P., Feichter, J., Kloster, S., Esch, M. and Fischer-Bruns, I.: Impact of carbonaceous aerosol
746   emissions on regional climate change, Clim. Dyn., 27(6), 553–571, doi:10.1007/s00382-006-0147-3, 2006.

747   Rotstayn, L. D. and Lohmann, U.: Tropical rainfall trends and the indirect aerosol effect, J. Clim., 15(15), 2103–
748   2116, doi:10.1175/1520-0442(2002)015<2103:TRTATI>2.0.CO;2, 2002.

749   Rosenfeld, D., Zhu, Y., Wang, M., Zheng, Y., Goren, T. and Yu, S.: Aerosol-driven droplet concentrations
750   dominate coverage and water of oceanic low-level clouds, Science (80-.)., 363(6427), eaav0566,
751   doi:10.1126/science.aav0566, 2019.

752   Samset, B. H., Myhre, G., Forster, P. M., Hodnebrog, Andrews, T., Faluvegi, G., Fläschner, D., Kasoar, M.,
753   Kharin, V., Kirkevåg, A., Lamarque, J. F., Olivié, D., Richardson, T., Shindell, D., Shine, K. P., Takemura, T.
754   and Voulgarakis, A.: Fast and slow precipitation responses to individual climate forcers: A PDRMIP multimodel
755   study, Geophys. Res. Lett., 43(6), 2782–2791, doi:10.1002/2016GL068064, 2016.

756   Samset, B. H., Myhre, G., Forster, P. M., Hodnebrog, Ø., Andrews, T., Boucher, O., Faluvegi, G., Fläschner, D.,

757   Kasoar, M., Kharin, V., Kirkevåg, A., Lamarque, J.-F., Olivié, D., Richardson, T. B., Shindell, D., Takemura, T.

758   and Voulgarakis, A.: Weak hydrological sensitivity to temperature change over land, independent of climate

759   forcing, npj Clim. Atmos. Sci., 1(1), 3, doi:10.1038/s41612-017-0005-5, 2017.

760   Shaw, T. A. and Voigt, A.: Tug of war on summertime circulation between radiative forcing and sea surface

761   warming, Nat. Geosci., 8(7), 560–566, doi:10.1038/ngeo2449, 2015.

762   Shawki, D., Voulgarakis, A., Chakraborty, A., Kasoar, M. and Srinivasan, J.: The South Asian Monsoon Response

763   to Remote Aerosols: Global and Regional Mechanisms, J. Geophys. Res. Atmos., 123(20), 11,585-11,601,

764   doi:10.1029/2018JD028623, 2018.

765   Stephens, G. L. and Hu, Y.: Are climate-related changes to the character of global-mean precipitation predictable?,

766   Environ. Res. Lett., 5(2), doi:10.1088/1748-9326/5/2/025209, 2010.

767   Stevens, B., Giorgetta, M., Esch, M., Mauritsen, T., Crueger, T., Rast, S., Salzmann, M., Schmidt, H., Bader, J.,

768   Block, K., Brokopf, R., Fast, I., Kinne, S., Kornblueh, L., Lohmann, U., Pincus, R., Reichler, T. and Roeckner,

769   E.: Atmospheric component of the MPI-M Earth System Model: ECHAM6, J. Adv. Model. Earth Syst., 5(2),

770   146–172, doi:10.1002/jame.20015, 2013.

771   Stier, P., Feichter, J., Kinne, S., Kloster, S., Vignati, E., Wilson, J., Ganzeveld, L., Tegen, I., Werner, M.,

772   Balkanski, Y., Schulz, M., Boucher, O., Minikin, A. and Petzold, A.: The aerosol-climate model ECHAM5-HAM,

773   Atmos. Chem. Phys., 5(4), 1125–1156, doi:10.5194/acp-5-1125-2005, 2005.

774   Stier, P., Seinfeld, J. H., Kinne, S., Feichter, J. and Boucher, O.: Impact of nonabsorbing anthropogenic aerosols

775   on clear-sky atmospheric absorption, J. Geophys. Res. Atmos., 111(18), 1–11, doi:10.1029/2006JD007147, 2006.

776   Stjern, C. W., Samset, B. H., Myhre, G., Forster, P. M., Hodnebrog, Ø., Andrews, T., Boucher, O., Faluvegi, G.,

777   Iversen, T., Kasoar, M., Kharin, V., Kirkevåg, A., Lamarque, J.-F., Olivié, D., Richardson, T., Shawki, D.,

778   Shindell, D., Smith, C. J., Takemura, T. and Voulgarakis, A.: Rapid Adjustments Cause Weak Surface

779   Temperature Response to Increased Black Carbon Concentrations, J. Geophys. Res. Atmos., 122(21), 11,462-

780   11,481, doi:10.1002/2017JD027326, 2017.

781   Stjern, C. W., Richardson, T., Myhre, G., Faluvegi, G., Olivié, D., Stier, P., Samset, B. H., Fläschner, D.,

782   Takemura, T., Lamarque, J.-F., Smith, C. J., Forster, P., Kirkevåg, A., Boucher, O., Soden, B. J., Voulgarakis, A.,

783   Shindell, D., Kasoar, M., Hodnebrog, Ø., Kramer, R. J., Andrews, T. and Watson-Parris, D.: Quantifying the

784   Importance of Rapid Adjustments for Global Precipitation Changes, Geophys. Res. Lett., 45(20), 11,399-11,405,

785   doi:10.1029/2018gl079474, 2018.

786   Suzuki, K. and Takemura, T.: Perturbations to Global Energy Budget Due to Absorbing and Scattering Aerosols,

787   J. Geophys. Res. Atmos., 124(4), 2194–2209, doi:10.1029/2018JD029808, 2019.

788   Suzuki, K., Stephens, G. L. and Golaz, J.-C.: Significance of aerosol radiative effect in energy balance control on

789   global precipitation change, Atmos. Sci. Lett., 18(10), 389–395, doi:10.1002/asl.780, 2017.

790 Tegen, I., Neubauer, D., Ferrachat, S., Drian, C. S. Le, Bey, I., Schutgens, N., Stier, P., Watson-Parris, D., Stanelle,
791 T., Schmidt, H., Rast, S., Kokkola, H., Schultz, M., Schroeder, S., Daskalakis, N., Barthel, S., Heinold, B. and
792 Lohmann, U.: The global aerosol-climate model echam6.3-ham2.3 -Part 1: Aerosol evaluation, Geosci. Model
793 Dev., 12(4), 1643–1677, doi:10.5194/gmd-12-1643-2019, 2019.

794 Tiedtke, M.: A Comprehensive Mass Flux Scheme for Cumulus Parameterization in Large-Scale Models, Mon.
795 Weather Rev., 117(8), 1779–1800, doi:10.1175/1520-0493(1989)117<1779:ACMFSF>2.0.CO;2, 1989.

796 van Marle, M. J. E., Kloster, S., Magi, B. I., Marlon, J. R., Daniau, A.-L., Field, R. D., Arneth, A., Forrest, M.,
797 Hantson, S., Kehrwald, N. M., Knorr, W., Lasslop, G., Li, F., Mangeon, S., Yue, C., Kaiser, J. W. and van der
798 Werf, G. R.: Historic global biomass burning emissions for CMIP6 (BB4CMIP) based on merging satellite
799 observations with proxies and fire models (1750–2015), Geosci. Model Dev., 10(9), 3329–3357,
800 doi:10.5194/gmd-10-3329-2017, 2017.

801 Wang, C.: The sensitivity of tropical convective precipitation to the direct radiative forcings of black carbon
802 aerosols emitted from major regions, Ann. Geophys., 27(10), 3705–3711, doi:10.5194/angeo-27-3705-2009,
803 2009.

804 Wang, H., Xie, S. P., Kosaka, Y., Liu, Q. and Du, Y.: Dynamics of Asian summer monsoon response to
805 anthropogenic aerosol forcing, J. Clim., 32(3), 843–858, doi:10.1175/JCLI-D-18-0386.1, 2019.

806 Wang, M., Ghan, S., Liu, X., L'Ecuyer, T. S., Zhang, K., Morrison, H., Ovchinnikov, M., Easter, R., Marchand,
807 R., Chand, D., Qian, Y. and Penner, J. E.: Constraining cloud lifetime effects of aerosols using A-Train satellite
808 observations, Geophys. Res. Lett., 39(15), 3–9, doi:10.1029/2012GL052204, 2012.

809 Wang, Z., Lin, L., Yang, M., Xu, Y. and Li, J.: Disentangling fast and slow responses of the East Asian summer
810 monsoon to reflecting and absorbing aerosol forcings, Atmos. Chem. Phys., 17(18), 11075–11088,
811 doi:10.5194/acp-17-11075-2017, 2017.

812 White, B., Gryspeerdt, E., Stier, P., Morrison, H., Thompson, G. and Kipling, Z.: Uncertainty from the choice of
813 microphysics scheme in convection-permitting models significantly exceeds aerosol effects, Atmos. Chem. Phys.,
814 17(19), 12145–12175, doi:10.5194/acp-17-12145-2017, 2017.

815 Zanis, P., Akritidis, D., Georgoulias, A. K., Allen, R. J., Bauer, S. E., Boucher, O., Cole, J., Johnson, B., Deushi,
816 M., Michou, M., Mulcahy, J., Nabat, P., Olivié, D., Oshima, N., Sima, A., Schulz, M., Takemura, T. and
817 Tsigaridis, K.: Fast responses on pre-industrial climate from present-day aerosols in a CMIP6 multi-model study,
818 Atmos. Chem. Phys., 20(14), 8381–8404, doi:10.5194/acp-20-8381-2020, 2020.

819 Zelinka, M. D., Myers, T. A., McCoy, D. T., Po-Chedley, S., Caldwell, P. M., Ceppi, P., Klein, S. A. and Taylor,
820 K. E.: Causes of Higher Climate Sensitivity in CMIP6 Models, Geophys. Res. Lett., 47(1), 1–12,
821 doi:10.1029/2019GL085782, 2020.

822 Zhang, K., O'Donnel, D., Kazil, J., Stier., P., Kinne, S., Lohmann, U., Ferrachat, S., Croft, B., Quaas, J., Wan,
823 H., Rast, S. and Feichter, J.: The global aerosol-climate model ECHAM-HAM, version 2: sensitivity to

824 improvements in process representations, Atmos. Chem. Phys., 12(19), 8911–8949, doi:10.5194/acp-12-8911-
825 2012, 2012.

826 Zhang, S: On the Contribution of Fast and Slow Responses to Precipitation Changes Caused by Aerosol
827 Perturbations, Mendeley Data, V1, doi: 10.17632/8n2vj578r2.1, 2021

828 Zhang, S., Wang, M., J. Ghan, S., Ding, A., Wang, H., Zhang, K., Neubauer, D., Lohmann, U., Ferrachat, S.,
829 Takeamura, T., Gettelman, A., Morrison, H., Lee, Y., T. Shindell, D., G. Partridge, D., Stier, P., Kipling, Z. and
830 Fu, C.: On the characteristics of aerosol indirect effect based on dynamic regimes in global climate models, Atmos.
831 Chem. Phys., 16(5), 2765–2783, doi:10.5194/acp-16-2765-2016, 2016.

832 Zhao, S. and Suzuki, K.: Differing Impacts of Black Carbon and Sulfate Aerosols on Global Precipitation and the
833 ITCZ Location via Atmosphere and Ocean Energy Perturbations, J. Clim., 32(17), 5567–5582, doi:10.1175/jcli-
834 d-18-0616.1, 2019.

835 Zheng, B., Tong, D., Li, M., Liu, F., Hong, C., Geng, G., Li, H., Li, X., Peng, L., Qi, J., Yan, L., Zhang, Y., Zhao,
836 H., Zheng, Y., He, K. and Zhang, Q.: Trends in China's anthropogenic emissions since 2010 as the consequence
837 of clean air actions, Atmos. Chem. Phys., 18(19), 14095–14111, doi:10.5194/acp-18-14095-2018, 2018.

838
839
840

841

Table 1. ECHAM6-HAM2 simulated multi-annual global averaged fast, slow, and total responses of atmospheric energy budget terms (LP – the atmospheric latent heating rate from rainfall, ARC – atmospheric radiative cooling, SH – sensible heat flux) and surface temperature (T) in response to increase of 10 times black carbon (BC) emission and 5 times sulphate (SUL) emission. ARC has been further decomposed into the contribution from aerosols, clouds and clear-clean sky. All of terms are shown in equivalent precipitation units of mm d^{-1}.

847

(mm d^{-1})	LΔP	ΔARC	ΔARC$_{aerosol}$	ΔARC$_{cloud}$	ΔARC$_{cc}$	-ΔSH	ΔT (K)
fast, 10BC	-0.13	-0.21	-0.29	0.03	0.05	0.08	-0.03
slow, 10BC	0.01	0.02	-0.01	0.00	0.04	-0.01	0.39
total, 10BC	-0.11	-0.18	-0.30	0.03	0.09	0.07	0.35
fast, 5SUL	-0.01	-0.01	0.01	0.00	-0.02	0.00	-0.14
slow, 5SUL	-0.14	-0.13	0.00	0.02	-0.15	-0.01	-1.73
total, 5SUL	-0.15	-0.14	0.01	0.01	-0.17	-0.01	-1.87

848

849

850

851

852
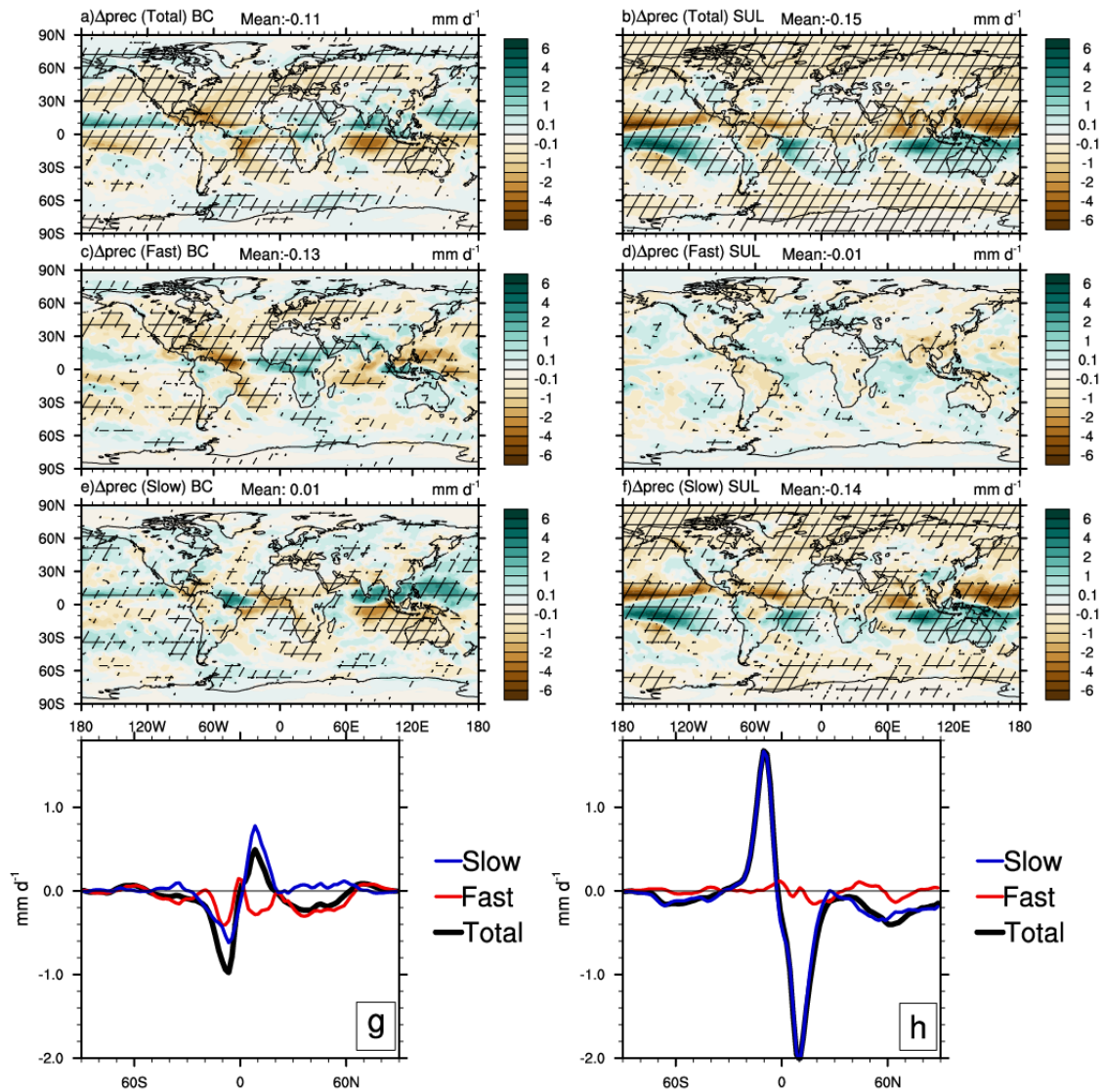
Figure 1. ECHAM6-HAM2 simulated geographical patterns of multi-annual mean precipitation change in response to increasing (left column) 10 times BC emissions and (right column) 5 times SUL emissions for (first row) total, (second row) fast, and (third row) slow responses. Hatching indicates where the changes are significant (90% confidence). (fourth row) Zonal averages of changes in precipitation in terms of total, fast and slow responses to increasing (g) 10 times BC emission and (h) 5 times SUL emission.

869

870
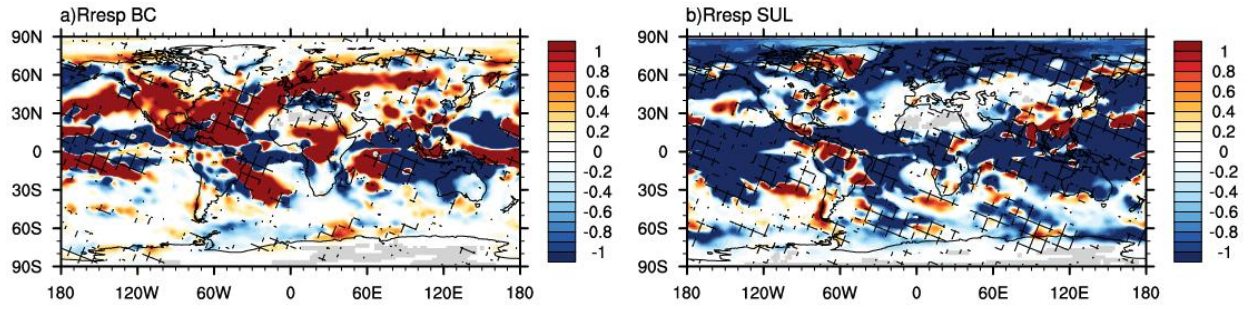
Figure 2. Response ratio of fast and slow responses (R_{resp}) (red denotes fast responses dominates the total responses and blue indicate slow responses dominates) of fast and slow responses for (a) BC cases and (b) SUL cases. Results have been normalised by total responses of precipitation. Hatching indicates the signs of fast and slow responses are same. If R_{resp} is around 0, contributions from fast and slow responses are similar. If R_{resp} is larger than 0, the total response is dominated by fast responses. If R_{resp} is less than 0, the total response is dominated by slow responses.

877

878

Figure 3. ECHAM6-HAM2 simulated geographical patterns of multi-annual mean changes in (first row) atmospheric diabatic cooling (ΔQ) and (second row) dry static energy flux divergence (ΔH) for (left column) fast responses and (right column) slow responses to 10 times BC emission. Hatching indicates where the changes are significant (90% confidence interval through bootstrapping methods). (e) The zonal mean of total precipitation response and its decompositions, including fast and slow responses of diabatic cooling and dry static energy flux divergence. All of them are shown in equivalent precipitation units of mm d^{-1}.

882
883
884
885
886
887
888

889
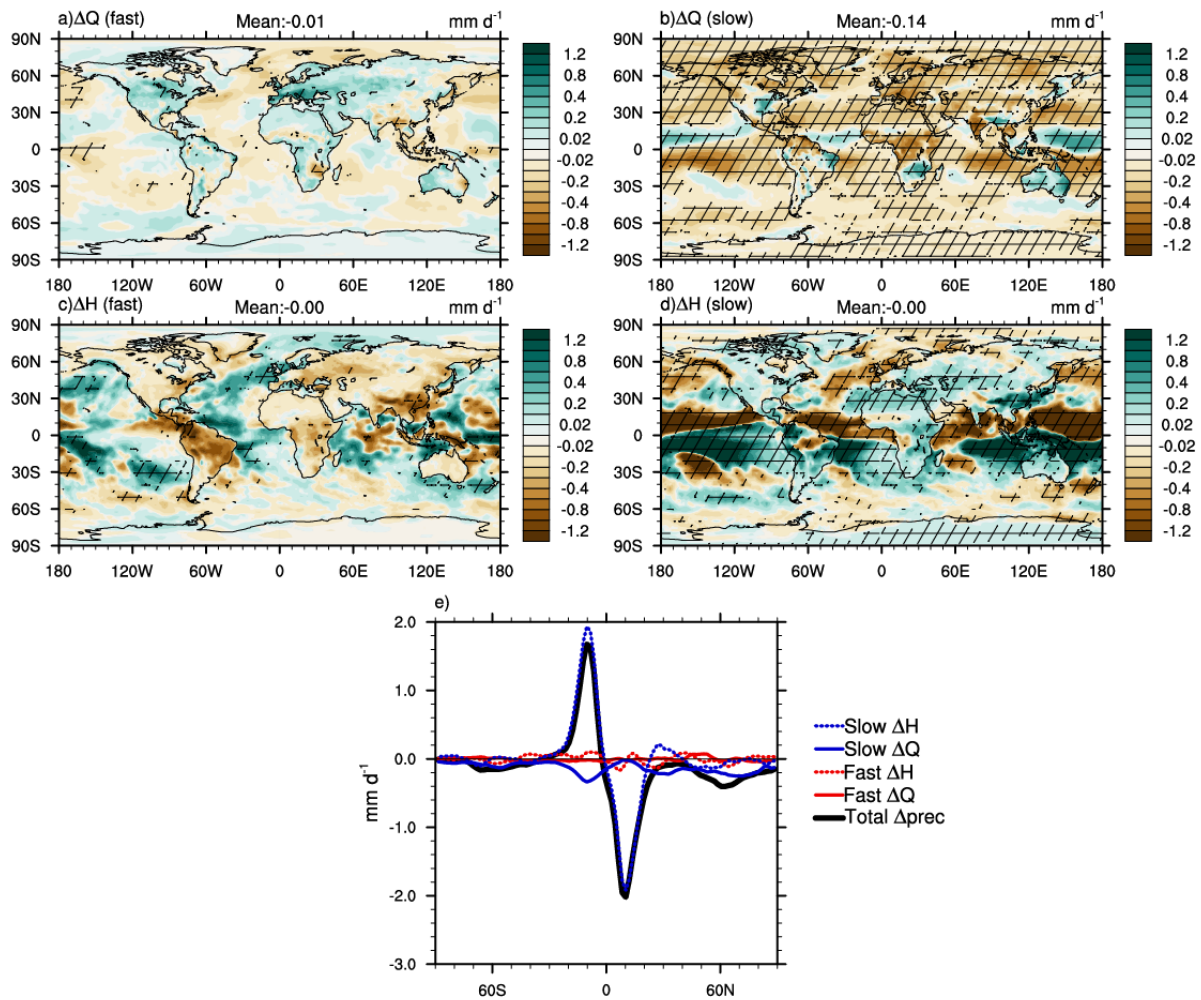
Figure 4. ECHAM6-HAM2 simulated geographical patterns of multi-annual mean changes in (first row) atmospheric diabatic cooling and (second row) dry static energy flux divergence for (left column) fast responses and (right column) slow responses to 5 times SUL emission. Hatching indicates where the changes are significant (90% confidence interval through bootstrapping methods). (e) The zonal mean of total precipitation response and its decompositions, including fast and slow responses of diabatic cooling and dry static energy flux divergence. All of them are shown in equivalent precipitation units of mm d⁻¹.

893
894
895
896
897
898
899

900

901

902
903
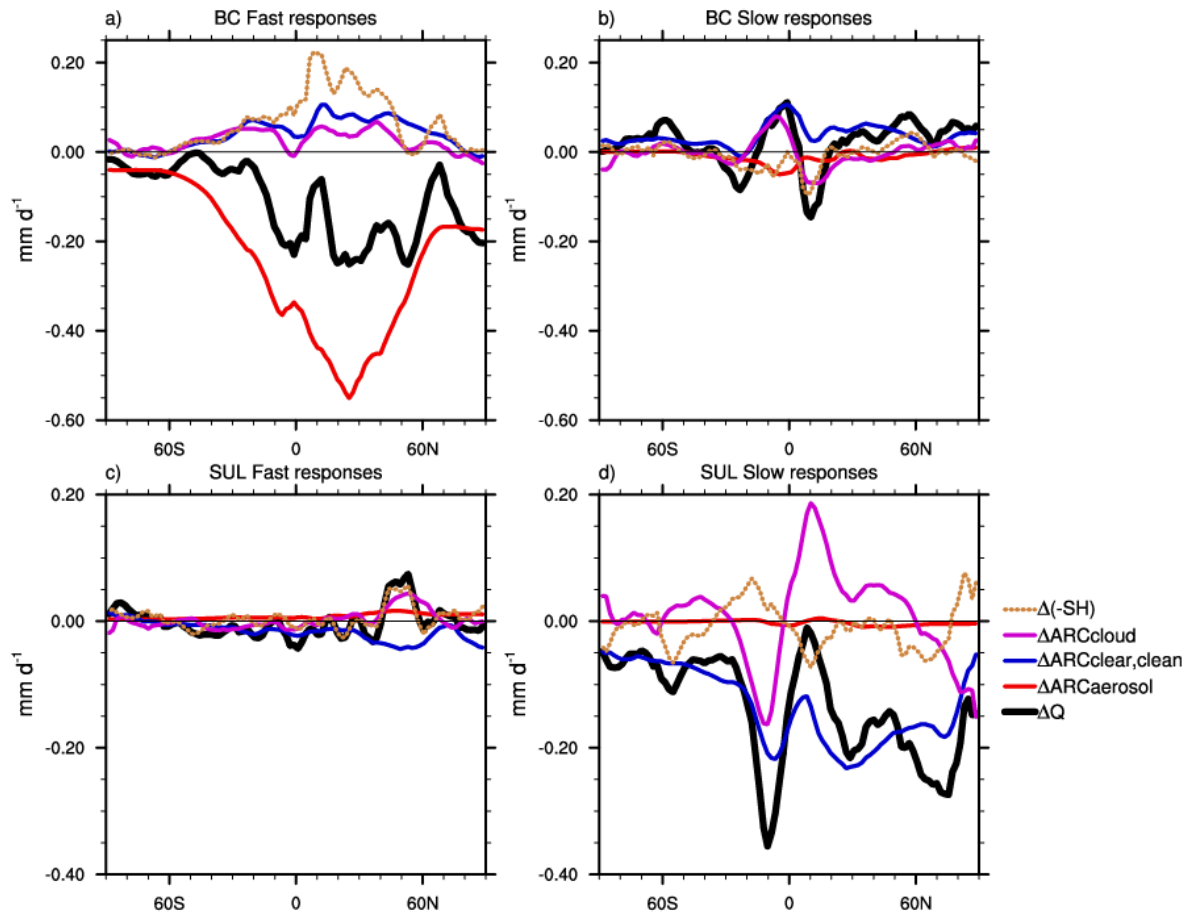
904
905 **Figure 5. ECHAM6-HAM2 simulated multi-annual zonal mean of decomposed changes in atmospheric diabatic cooling**
906 **(ΔQ), including ARC changes from aerosols ($\Delta ARC_{aerosol}$), clouds (ΔARC_{cloud}), clear-clean sky ($\Delta ARC_{clear,clean}$),**
907 **downward sensible heat flux($\Delta(-SH)$) for (a) fast responses in the BC case, (b) slow responses in the BC case, (c) fast**
908 **responses in the SUL case, and (d) slow responses in the SUL case. All items are shown in equivalent precipitation units**
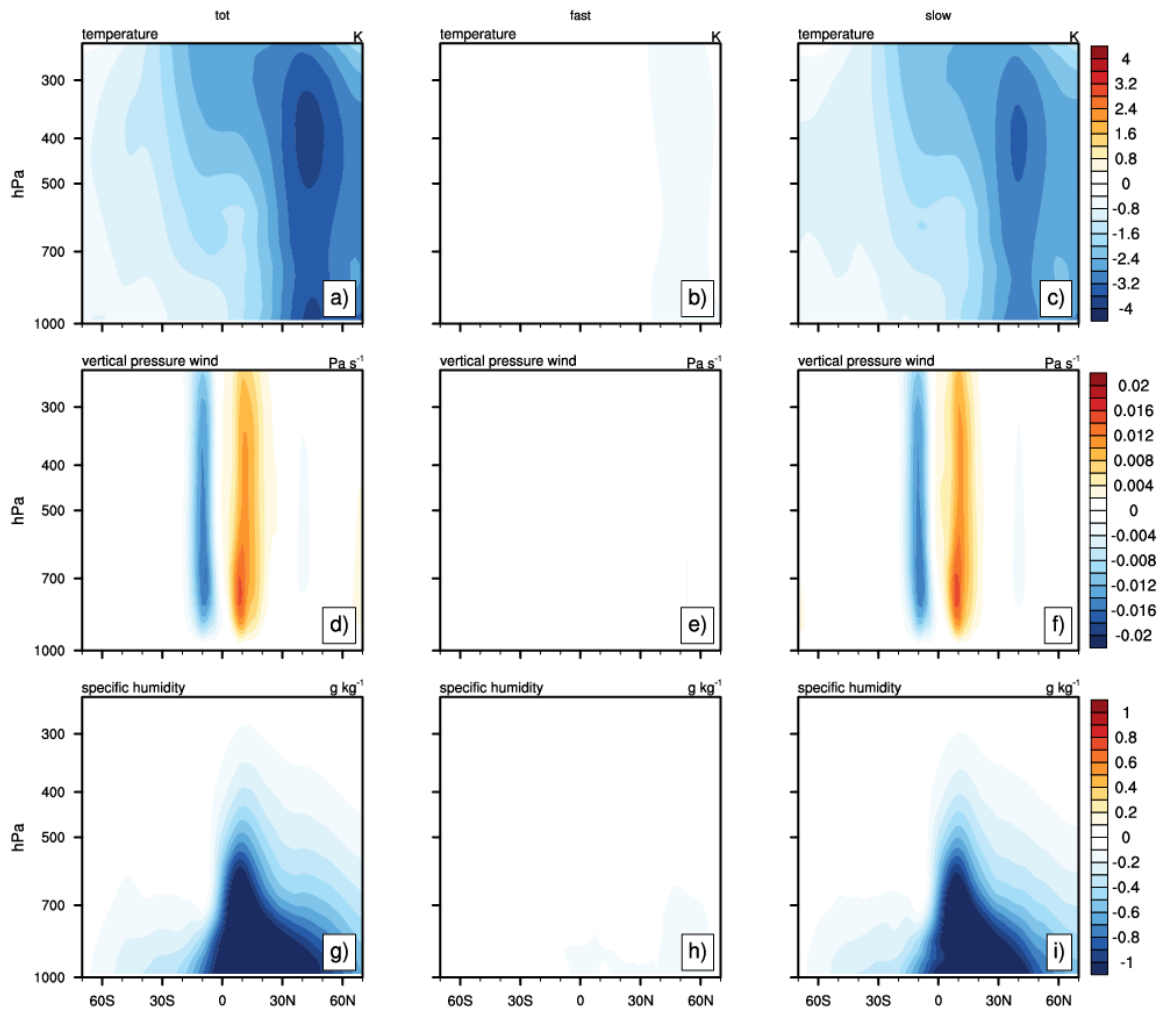909 **of mm d^{-1}.**

910
911
912

913
914
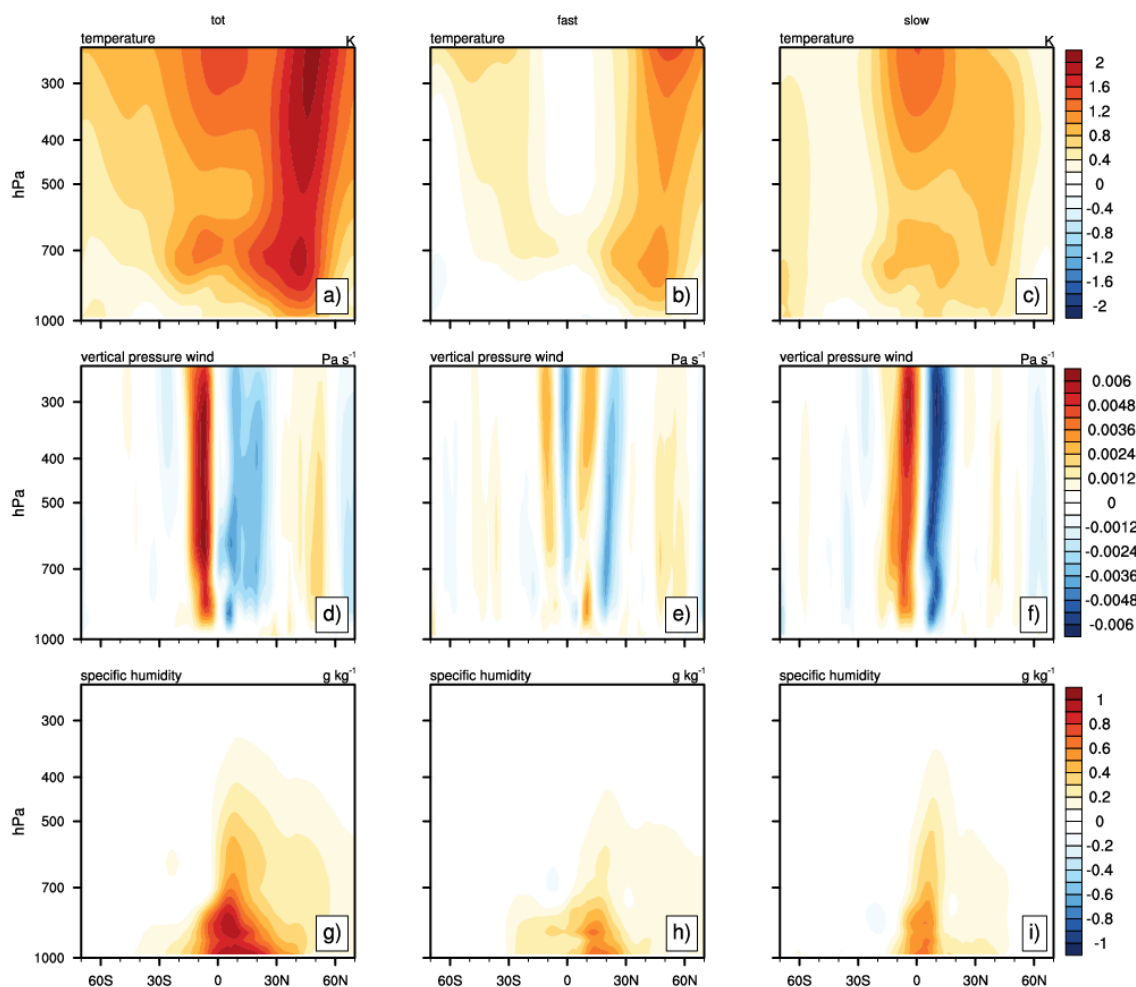
915
916 **Figure 6. ECHAM6-HAM2 simulated multi-annual (left column) total, (middle column) fast, and (right column) slow**
917 **responses of zonally averaged (a, b, c) temperature, (d, e, f) vertical pressure velocity, and (g, h, i) specific humidity in**
918 **response to 10 times BC emission. Blue colours indicate large-scale ascent, and red colours indicate large-scale descent**
919 **in d-f.**

920
921

922
923
924

925
926

Figure 7. ECHAM6-HAM2 simulated multi-annual (left column) total, (middle column) fast, and (right column) slow responses of zonally averaged (a, b, c) temperature, (d, e, f) vertical pressure velocity, and (g, h, i) specific humidity in response to 5 times SUL emission. Blue colour indicates large-scale ascent, and red colour indicates large-scale descent in d-f.

931

932
933